Zambri Brian (Orcid ID: 0000-0002-1497-1954)
Robock Alan (Orcid ID: 0000-0002-6319-5656)
Mills Michael James (Orcid ID: 0000-0002-8054-1346)
Schmidt Anja (Orcid ID: 0000-0001-8759-2843)

Modeling the 1783–1784 Laki Eruption in Iceland, Part II: Climate Impacts

Brian Zambri[1,2], Alan Robock[1], Michael J. Mills[3], and Anja Schmidt[4,5]

[1]Department of Environmental Sciences, Rutgers University, New Brunswick, NJ, USA
[2]Now at: Department of Earth, Atmospheric, and Planetary Sciences, Massachusetts Institute of Technology, Cambridge, MA, USA
[3]Atmospheric Chemistry Observations and Modeling Laboratory, National Center for Atmospheric Research, Boulder, CO, USA
[4]Department of Chemistry, University of Cambridge, Lensfield Road, Cambridge CB2 1EW, UK
[5]Department of Geography, University of Cambridge, Downing Place, Cambridge CB2 3EN, UK

Key Points:

- The July 1783 heatwave in Western Europe was likely caused by anomalous circulation, and not caused by the Laki eruption.

- Africa and Asia faced large reductions in precipitation after the Laki eruption, which caused widespread drought and famine.

- The Laki eruption increased the likelihood of an El Niño in the subsequent boreal winter.

Correspondence to:

Brian Zambri
Department of Earth, Atmospheric, and Planetary Sciences
Massachusetts Institute of Technology
77 Massachusetts Avenue
Cambridge, MA 02139
Email: bzambri@mit.edu

ABSTRACT

The Laki eruption in Iceland, which began in June 1783, was followed by many of the typical climate responses to volcanic eruptions: suppressed precipitation and drought, crop failure, and surface cooling. In contrast to the observed cooling in 1784–1786, the summer of 1783 was anomalously warm in Western Europe, with July temperatures reaching more than 3 K above the mean. However, the winter of 1783–1784 in Europe was as cold as 3 K below the mean. While climate models generally reproduce the surface cooling and decreased rainfall associated with volcanic eruptions, model studies have failed to reproduce the extreme warming in western Europe that followed the Laki eruption. As a result of the inability to reproduce the anomalous warming, the question remains as to whether this phenomenon was a response to the eruption, or merely an example of internal climate variability. Using the Community Earth System Model from the National Center for Atmospheric Research, we investigate the "Laki haze" and its effect on Northern Hemisphere climate in the 12 months following the eruption onset. We find that the warm summer of 1783 was a result of atmospheric blocking over Northern Europe, that in our model cannot be attributed to the eruption. In addition, the extremely cold winter of 1783–1784 was aided by an increased likelihood of an El Niño after the eruption. Understanding the causes of these anomalies is important not only for historical purposes, but also for understanding and predicting possible climate responses to future high-latitude volcanic eruptions.

1. Introduction

Volcanic eruptions can have global climate impacts lasting several years. When large, explosive eruptions inject sulfur gases into the stratosphere, they are converted to sulfate aerosols, which attenuate incoming shortwave (SW) solar radiation, resulting in a cooling of Earth's surface [*Robock and Mao*, 1995; *Robock*, 2000]. High-latitude eruptions have more limited impacts on global climate than tropical eruptions of the same or similar size, because the atmospheric circulation tends to cause the aerosol plume to remain in the hemisphere in which the eruption occurs [*Schneider et al.*, 2009; *Kravitz and Robock*, 2011; *Jones et al.*, 2017]. An exception to this tendency could occur in summer in the case of volcanic sulfur injected into the upper stratosphere or mesosphere, where sulfur would exist as a gas and be transported to the opposing hemisphere, and could form aerosols on descent the middle and lower stratosphere [e.g., *Butchart*, 2014]. One high-latitude eruption that is often studied is the 1783–1784 Laki eruption in Iceland, which was unique in that the basaltic flood lava eruption injected sulfur gas into the lower troposphere as well as into the lower stratosphere [*Thordarson and Self*, 1993, 2003; *Thordarson et al.*, 1996, 2003]. In addition to a constant effusing of gas from the Laki lava flows in the troposphere from June 8, 1783, to February 7, 1784, Laki was characterized by 10 explosive phases that injected sulfur gas into the upper troposphere and lower stratosphere at an altitude of 9–13 km; stratospheric injection of SO_2 for these explosive episodes ranged from 2.9 to 18.7 Tg [Table 1; *Thordarson and Self*, 2003]. Because of the unique nature of this eruption, its impacts on climate and atmospheric composition have been studied extensively using models of various types [*Highwood and Stevenson*, 2003; *Stevenson et al.*, 2003; *Oman et al.*, 2006a, 2006b; *Kravitz and Robock*, 2011; *Pausata et al.*, 2015a, 2015b, 2016; *Schmidt et al.*, 2010, 2012].

There are many contemporary reports of the sulfuric aerosol cloud that lingered over most of the Northern Hemisphere (NH) in 1783, with various explanations proposed for the

"Laki haze." Earthquakes in Calabria, which occurred during the first half of 1783, were a common explanation [*Hamilton*, 1783; *van Swinden*, 1783; *Thordarson and Self*, 2003 and references therein]. *De Montredon* [1784] is credited with being the first to tie the dry fog in Europe to volcanic activity in Iceland, and his more famous contemporary Benjamin Franklin proposed a similar explanation after de Montredon, attributing the fog to Hekla, a volcano in Iceland that did not erupt that year:

> "During several of the summer months of the year 1783, when the effect of the sun's rays to heat the earth in these northern regions should have been greatest, there existed a constant fog over all Europe, and great part of North America…whether it was the vast quantity of smoke, long continuing to issue during the summer from Hecla [sic] in Iceland, and that other volcano which arose out of the sea near that island, which smoke might be spread by various winds, over the northern part of the world, is yet uncertain." [*Franklin*, 1784]

The atmospheric pollution by the Laki haze caused environmental stress and health hazards across Iceland and Europe [*Grattan et al.*, 2003; *Thordarson and Self*, 2003]. Reports from across Europe included visibility reductions and the smell of sulfur or hydrogen sulfide. The air pollution resulted in "troublesome headaches, respiratory difficulties, and asthma attacks," as well as damage to trees and crops due to acid rain [*van Swinden*, 1783; *Thordarson and Self*, 2003]. In Iceland, more than 60% of the livestock perished within a year, and the ensuing famine caused the death of about 20% of the human population [*Thordarson and Self*, 2003]. In addition, parish records for the summer of 1783 in England suggest extremely high mortality rates [*Grattan et al.*, 2003; *Schmidt et al.*, 2011]. Historical accounts of increased mortality rates and/or respiratory disorders are also found across Europe [*Schmidt et al.*, 2011, and references therein].

Along with the direct health hazards from the Laki haze, the eruption was followed by abrupt and unique regional climate change in the years following: the summer after the eruption was extremely warm in Europe, most of the NH experienced extreme cold that winter [*Thordarson and Self*, 2003; *Luterbacher et al.*, 2004; *Schmidt et al.*, 2012], and Africa and Asia experienced extreme drought, crop failure, and famine for several years [*Wood*, 1992; *Oman et al.*, 2006a]. While surface cooling and reductions of tropical precipitation are expected impacts of a volcanic eruption and have been reproduced by model studies in the past [e.g., *Oman et al.*, 2006a,b; *Schmidt et al.*, 2012; *Pausata et al.*, 2015b], the European heat wave in July 1783 has yet to be explained or reproduced. It has been proposed that the anomalously high temperatures were due to greenhouse warming by sulfur gases in the troposphere that made their way to Europe from Iceland [*Grattan and Sadler*, 1999], though this effect was shown to be quite small when compared to the negative radiative forcing caused by the volcanic aerosols [*Highwood and Stevenson*, 2003]; others have posited that the warming was merely an example of climate variability [*Thordarson and Self*, 2003].

D'Arrigo et al. [2011] argued that internal variability in the form of a concurrent El Niño and negative phase of the North Atlantic Oscillation (NAO), and not the Laki eruption, was responsible for the extremely cold winter of 1783-1784. The NAO is an index of the wintertime variability of north-south NH sea level pressure gradients between 110°W and 70°E and north of 20°N [*van Loon and Rogers*, 1978; *Hurrell*, 1995; *Christiansen*, 2008], and has been associated with an anomalously strong polar vortex [e.g., *Kodera et al.*, 1991; *Perlwitz and Graf*, 1995; *Thompson and Wallace*, 1998]. While observations [*Christiansen*, 2008] and models [*Bittner et al.*, 2016a, 2016b; *Zambri and Robock*, 2016; *Zambri et al.*, 2017] have shown a tendency toward a strengthened polar vortex and a positive NAO in the first winter after large tropical volcanic eruptions, the circulation response to high-latitude

eruptions is less well understood. Using the Goddard Institute for Space Studies ModelE general circulation model, *Oman et al.* [2005] found a weak negative NAO-like pattern after the 1912 Katmai eruption in Alaska, due to stratospheric heating by volcanic aerosols and a subsequent weakening of the polar vortex. However, it is unclear whether this is a robust response, and whether there is enough solar radiation near the pole in the NH wintertime to overcome the high level of internal variability and elicit a dynamical response; for example, *Kravitz and Robock* [2011] found little impact on NH winter surface air temperature from a high-latitude eruption similar in magnitude to Katmai (5 Tg SO_2).

In contrast to the claim that the 1783–1784 El Niño also occurred by chance, a model study using the Norwegian Earth System Model 1 [NorESM1-M; *Bentsen et al.*, 2013], *Pausata et al.* [2015a, 2016] simulated an increase in the likelihood of an El Niño in the first year after large, high-latitude eruptions. They hypothesized that the southward shift of the Inter-Tropical Convergence Zone (ITCZ) due to preferential cooling in the NH [*Colose et al.*, 2016] generates anomalous westerly winds at the surface of the central and western equatorial Pacific and equatorial northerlies in the eastern pacific, priming the Pacific Ocean for an El Niño-like perturbation [*Pausata et al.*, 2015a]. *Pausata et al.* [2016] examined the role of initial conditions, and found that the largest anomalies are simulated after an eruption that occurs during a developing La Niña or El Niño/Southern Oscillation (ENSO)-neutral conditions. They attribute this result to the fact that the ITCZ is farther north and the equatorial trade winds stronger in La Niña and neutral conditions than in El Niño conditions.

We use the National Center for Atmospheric Research's Community Earth System Model, version 1 [CESM1; *Hurrell et al.*, 2013], with the Whole Atmosphere Community Climate Model [WACCM; *Marsh et al.*, 2013], to conduct an ensemble of simulations of the Laki eruption in Iceland. In a complementary study [*Zambri et al.*, 2018a], we analyzed the evolution of the Laki aerosol cloud and its effects on atmospheric circulation and

composition. Here, we aim to diagnose the abnormally warm summer and extremely cold winter either as consequences of Laki or not; this information can be used to forecast the climate impacts of a future large high-latitude eruption. The rest of the paper is structured as follows: in Section 2 we describe the CESM1(WACCM) model and experimental setup of the Laki simulations; in Section 3 we present the results, including analysis of the radiative forcing and the evolution of the Laki aerosol cloud, the summer climate response to the Laki eruption, and the winter climate response; Section 4 contains a summary and discussion of the results.

2. Model Description and Experiment Setup

CESM1 is composed of interactive atmosphere, ocean, land, and sea ice components. For these experiments, we used WACCM, the high-top atmospheric component of CESM1 [*Marsh et al.*, 2013]. The version of WACCM used here is that described by *Mills et al.* [2017], which includes more realistic formulations of radiation, cloud microphysics, and aerosols. The model has 70 vertical levels, a model top of 5.1 x 10^{-6} hPa and 0.9° latitude x 1.25° longitude horizontal resolution, with interactive atmospheric chemistry, radiation, and dynamics. Direct effects of aerosols are included in the radiation code and indirect effects of sulfur are included in the cloud microphysics [*Morrison and Gettelman*, 2008; *Gettelman et al.*, 2010].

Aerosols are represented in WACCM using a three-mode prognostic modal aerosol model [MAM3; *Liu et al.*, 2012], which represents the aerosols in Aitken, accumulation, and coarse modes. MAM3 has been modified to simulate the evolution of stratospheric sulfate aerosols from volcanic and non-volcanic emissions [*Mills et al.*, 2016]. MAM3 is capable of representing aerosol microphysical processes, such as nucleation, condensation, coagulation, and sedimentation, and calculates new particle formation using a parameterization of sulfuric acid–water homogeneous nucleation [*Vehkamäki et al.*, 2002].

Simulations follow the emissions budget detailed in *Thordarson and Self* [2003]. We inject 122 Tg of SO_2 into the atmosphere over 8 months beginning on June 8, 1783. About 94 Tg of SO_2 were injected into the upper troposphere/lower stratosphere between 9 and 13 km (Table 1), with another 28 Tg of SO_2 emitted at the surface from lava degassing (Table 2). About 95% of the total SO_2 emission took place in the first 4 months of activity, with the last explosive episode occurring in October 1783. The remainder of the emissions were due to the quiet emission of lava and gas over the last 4 months [Figure 2 of *Thordarson and Self*, 2003]. We simulated the eruption by injecting 94 Tg of SO_2 over ten eruptions from June 8 to October 25; the individual explosive eruption episodes range from injections of 2.9 to 18.7 Tg of SO_2 (Table 1). For each explosive episode, our simulated emissions occur over a 6-hour period from 1200 UTC to 1800 UTC. The SO_2 gas from the explosive episodes is evenly distributed within 5 vertical layers from 9 to 13 km. At the same time, we simulated SO_2 emitted by lava degassing by injecting an additional 28 Tg of SO_2 into the lowest model level from June 8, 1783 to February 7, 1784, continuously at the rates in Table 2.

Thordarson and Self [2003] determined that the transport of the Laki aerosols from Iceland to Europe was due to the circulation at the time of the eruption. Therefore, to initialize the model runs, we choose initial conditions that resembled the synoptic conditions reported over Europe around the time of the Laki eruption [Figure 1a; *Kington*, 1988; *Thordarson and Self*, 2003]. We choose four sets of initial conditions from a 25-year control run based on this criterion (Figure 1b–e). However, the background state of the global circulation was different for each set of initial conditions. In this way, it is possible to investigate the role of the background initial state in the impact of volcanic eruptions on climate. For example, we chose initial conditions with different ENSO phases to investigate the ENSO response to high-latitude eruptions.

For each set of initial conditions, we generated 10 ensemble members by perturbing the initial temperature field. We ran one 40-member ensemble with the Laki eruption (Laki) and one 40-member ensemble without the eruption (noLaki). Each simulation begins on June 8, the first day of the Laki eruption, and are run until June 1 of the following year. One set of chosen initial conditions from the control simulation features a strong El Niño event, similar to the winter of 1783–1784 during the Laki eruption [*Cook and Krusic*, 2004; *D'Arrigo et al.*, 2011].

Unless otherwise noted, anomalies were calculated by subtracting the mean of the 5 years before the eruption. We analyzed monthly means of model outputs, and we calculate the statistical significance of anomalies using the Student's *t*-test. Except where specifically stated, significance is reported at the 95% confidence level. We compared temperature responses to the average of 30 ensemble members from the latest reanalysis, the 400-year Ensemble Kalman Filter reanalysis [EKF400; *Franke et al.*, 2017]. EKF400 uses instrumental data series, reconstructed sea ice and temperature indices derived from documentary records, and proxy temperature reconstructions from Greenland ice cores and tree rings from Scandinavia and Siberia.

3. Results

3.1 Radiative Impacts

Figure 2 shows the zonally averaged volcanic effective radiative forcing (ERF) from the Laki eruption. We calculate the volcanic ERF as in *Schmidt et al.* [2018], and include contributions from aerosol-radiation interactions (ERF_ari), aerosol-cloud interactions (ERF_aci), and atmospheric adjustments and surface albedo forcing (dLW_ERFa). The SW radiation anomalies in Figure 2a indicate a maximum reduction of insolation – approximately 1 month after the eruption onset and lasting 2 months – of more than 31 W/m^2 poleward of 50ºN. The spatial and temporal location of this maximum is consistent with the latitude of the

eruption (64°N) and the timescale (weeks) for conversion of SO_2 to sulfate aerosols, the dominant driver of radiative effects from volcanic eruptions [*Robock*, 2000; *Kravitz and Robock*, 2011]. In addition, the maximum SW anomaly coincides with the maximum aerosol optical depth (AOD) perturbation and sulfate aerosol concentrations in the simulations [Figures 2, 4, respectively in *Zambri et al.*, 2018]. The radiative effects are strongly dependent on both time and latitude, with the SW anomalies above -1 W/m^2 and even changing signs by March 1784, and anomalies near the equator much weaker than at high latitudes; we discuss the positive SW anomalies in more detail below. At midlatitudes, the decrease in SW forcing is more gradual, and the steepest temporal gradient is seen at high latitudes, with anomalies reaching below -1 W/m^2 by November 1783; while the sulfate aerosol concentration at high latitudes begins decreasing by September 1783 [Figure 4 in *Zambri et al.*, 2018], a significant concentration remains into 1784, and the decrease in SW forcing is mostly due to a lack of insolation at high latitudes during boreal winter months.

Longwave (LW) forcing from the volcanic aerosols shows a similar spatial and temporal pattern (Figure 2b). The maximum decrease of 15 W/m^2 in outgoing LW radiation occurs at high latitudes in July and persists into August. In contrast to the SW anomalies, the LW forcing at high latitudes persists into the winter months; because of their independence on the seasonality of incoming solar radiation, the LW anomalies in Figure 2a show a timeline more consistent with the AOD and sulfate aerosol perturbations in *Zambri et al.* [2018]. North of 20ºN, LW anomalies persist into April and May 1784, while the anomalies change sign at and below 20ºN in 1784.

Figure 2c shows the net ERF due to the volcanic eruption, which is simply the linear combination of Figures 2a and 2b. At high latitudes, the large negative forcing is short-lived, with LW anomalies dominating in the winter for reasons discussed above, and positive SW anomalies in the following spring. Anomalies at midlatitudes follow a similar pattern, but

with a more gradual transition from negative to positive forcing. At 10–30ºN, a smaller negative forcing between –5 and –1 W/m^2 persists into May 1784; a positive anomaly of similar magnitude is simulated from 0–10ºN.

As mentioned previously, the volcanic ERF in Figure 2 contains contributions from aerosol-radiation interactions, aerosol-cloud interactions, and atmospheric adjustment and surface albedo forcing. In Figure 3a, the NH-average net volcanic ERF, along with each of its three components (ERF_ari, ERF_aci, and dLW_ERFa) are plotted. The NH-average ERF peaks with a value below –10 W/m^2 in July 1873 (Figure 3a). About two-thirds of this anomaly is due to aerosol-radiation interactions (red line, ~–6 W/m^2 in July 1783), with aerosol-cloud interactions (blue line) and dLW_ERFa (green line) contributing about –2.5 and –1.5 W/m^2, respectively. This large, negative forcing is accompanied by cooling of more than 1 K in the NH-average in October (Figure 3b). Beginning in November 1783, the net radiative forcing from the Laki eruption is in fact positive, and reaches 3 W/m^2 in May 1783, with the main contribution coming at this point from aerosol-cloud interactions.

As expected, the largest contributions to the volcanic ERF come from aerosol-radiation interactions, with the NH-average anomaly peaking at –6 W/m^2 in July and August 1783 and decreasing to about 0.5 W/m^2 by January 1784; this small-but-persistent anomaly lasts into May 1784. The next-largest contributor to the Laki volcanic ERF is aerosol-cloud interactions, with peak negative forcing of about –2.5 W/m^2 in July 1783; this forcing is caused by a large increase in cloud droplet number concentration in low clouds, which makes these clouds less transparent to incoming SW radiation (Figure S1a). In August 1783, the cloud forcing anomaly changes signs and steadily increases to a maximum forcing above 4 W/m^2 in May 1784. At higher altitudes, the dominating cloud effect is an increase in ice crystal number concentration (Figure S1b), which has a net heating effect, acting to trap more LW radiation that would otherwise escape to space. Atmospheric adjustments and surface

albedo forcing contribute the least to the ERF, with a local minimum of about -1.5 W/m^2 in July 1783, increasing to about 1 W/m^2 in October 1783, and decreasing once again to about $-$0.5 W/m^2 from February 1784 onward. The spatial and temporal patterns in Figures 2 and 3 are in general agreement with past modeling studies of the Laki eruption [e.g., *Oman et al.*, 2006b]. However, the anomalies in this study are found to be lower in magnitude than those in *Oman et al.* [2006b] and *Pausata et al.* [2015b]. This is most likely due to different treatments of volcanic aerosols in the models, which is discussed by *Zambri et al.* [2018]. In particular, simulations in *Pausata et al.* [2015b] extended the tropospheric aerosol scheme upward in order to simulate prognostic aerosols in the stratosphere; as a result, they simulate smaller particle sizes which scatter light more efficiently per unit mass than the larger-sized particles in the simulations presented here. This can explain the discrepancies between the radiative forcing anomalies simulated here and in previous studies; however, differences in radiation schemes in the models may also play a role.

We now return briefly to some of the anomalies pointed out in Figure 2. Specifically, there are somewhat unexpected and rather large positive SW anomalies at midlatitudes beginning in March 1784 (Figure 2a). From Figure 3a, it is clear that these anomalies are due to what are considered aerosol-cloud interactions (ERF_aci). However, by the time these positive anomalies appear in Figure 2a, the tropospheric aerosol concentration has returned to pre-eruption levels [Figure 4 in *Zambri et al.,* 2018]. As shown in Figure S1b, in-cloud ice crystal number concentration anomalies are everywhere below 0.005 cm^{-3} by February 1783. The quantity ERF_aci is a measure of the difference in cloud radiative forcing between the noLaki and Laki ensembles. This includes not only changes in cloud optical properties, but also changes in cloud cover in time and space between the two ensembles. Figure S2 shows the time series of low cloud and total cloud cover anomalies (Laki minus noLaki). These anomalies show reductions in low and total cloud cover coincident with the positive SW

anomalies in Figure 2a; this, along with Figure S1 and the lack of sulfate aerosol in the troposphere after February 1784 indicate that the positive forcing in Figures 2a and 3a are related to changes in the presence of clouds between the two ensembles, and not changes in microphysical properties of the clouds due to the Laki volcanic aerosol. However, both the cloud cover anomalies and the positive forcing are consistent across ensemble members.

3.2 Summer 1783

Figure 4 shows the JJA 1783 surface temperature anomalies for the EKF400 reanalysis and the Laki ensemble. The cooling in the EKF400 reanalysis (Figure 4a) is concentrated mostly over Northern Eurasia, Northeastern North America, and Alaska, and is below –3 K in some areas. Tree ring reconstructions show that the summer of 1783 was the coldest in hundreds of years in northwestern Alaska and northwest Siberia [*Jacoby et al.*, 1999; *Hantemirov et al.*, 2004]. These proxies, which are used to constrain the reanalysis, can help to explain why the cooling in Figure 5a is strongest in these areas. In contrast to the cooling, Western Europe shows significant warming, most likely related to the exceedingly warm conditions in July 1783 [*Thordarson and Self*, 2003]. The Laki ensemble (Figure 4b) simulates strong, significant cooling over the entire extratropics and NH high latitudes, with anomalies almost uniformly below –2 K for the summer, and reaching below –3 K. The magnitude and spatial pattern of cooling in Figure 4b is very similar to that found in Oman et al. [2006a].

In July 1783, an extreme heat wave hit northern, western and part of central Europe (Figure 5a). Historical reports indicate extreme warmth in Scandinavia [*Hólm*, 1784], while England experienced one of the warmest Julys on record in 1783 [*Manley*, 1974; *Kington*, 1978; *Parker et al.*, 1992]. The occurrence of this extreme heat coincides with the maximum LW radiative forcing in Figure 3b, and is also when the intensity of the Laki haze was the greatest in Western Europe [*Thordarson and Self*, 2003]. The EKF400 reanalysis (Figure 5a)

shows that in the western part of Europe the 1783 July surface temperatures are up to 1.5 K higher than the 1778–1782 mean, with temperatures were near or below the norm in the rest of Europe. No modeling study has been able to reproduce the observed warming and, as such, no mechanism relating the warm July of 1783 in Europe to the Laki eruption has materialized. Past studies have proposed that the July heat wave resulted from greenhouse warming caused by high SO_2 concentrations in the lower troposphere, emissions from Laki that did not convert to sulfate aerosols [*Wood*, 1992; *Rampino et al.*, 1995; *Grattan and Saddler*, 1999], but *Highwood and Stevenson* [2003] estimated that the magnitude of this positive radiative forcing would be less than 10% of the magnitude of the negative radiative forcing due to the sulfate aerosols. *Thordarson and Self* [2003], on the other hand, suggested that the unusually warm weather may have been caused by anomalous circulation over Europe, resulting in anomalous southerly winds. That is, the warm spell in the summer after Laki happened by chance, and was simply an example of internal climate variability. Similar heat waves have occurred recently in Europe without volcanic eruptions as precursors; the summer of 2003 was extremely warm and caused many heat-related deaths [*Stott et al.*, 2004].

The Laki ensemble mean (Figure 5b) shows significant cooling over all of Western Europe in JJA 1783, with anomalies reaching below –2.5 K in Central Europe. This response is consistent with the results in previous studies [e.g., *Oman et al.*, 2006a; *Pausata et al.*, 2015b], and is the expected response to a large, explosive volcanic eruption. On the other hand, the noLaki ensemble mean (Figure 5c) indicates significant warming over Europe, similar in magnitude to the EKF400 reanalysis shown in Figure 5a, though the warming in the noLaki ensemble is shifted northward. The warming seen in the noLaki ensemble is likely related to a decrease in low cloud cover and soil moisture in these simulations; indeed, Figure

S3 shows decreases of more than 25% in both these quantities, coincident with the maximum

warming over Northern Europe.

Of course, the observed "response" to the Laki eruption in Europe in July 1783 represents only one possible climate state after the volcanic eruption [*Kay et al.*, 2015]. Therefore, it is important to look at the individual simulated responses, and not just the mean response, which averages out internal climate variability and may never actually be realized. For this reason, Figure 6 shows the July 1783 surface temperature anomalies for each of the 40 simulations from the Laki ensemble. Several simulations (e.g., 1, 12, 15, 21) show large warming above 3 K over Northern and Western Europe in spite of the eruption. These individual simulations highlight the importance of the effects of internal variability on the subsequent climate state after the volcanic eruption.

That the summer response is not always simulated does not preclude the Laki eruption as the cause of the response. However, Figure 8 shows that this type of anomaly over Europe occurs even more frequently in the noLaki ensemble (e.g., 1–14, 16–20). The high frequency observed in Figure 7 does imply that the anomaly might be a result of circulation, and not specifically caused by the Laki eruption. To further investigate this, we analyzed the sea-level pressure and 850-hPa wind patterns associated with this type of anomaly. Similar analyses have been used in previous studies, e.g., to attribute decreased cloud droplet size over the North Atlantic region to aerosols from the 2014–2015 Holuhraun fissure eruption in Iceland [*Malavelle et al.*, 2017]. In Figure 8 we show the relationship between European temperatures and the atmospheric circulation in the surrounding area; we divided the Laki and noLaki ensembles into "blocking" and no "blocking" subsets, where members of the "blocking" subset are identified by high pressure over Northern Europe and low pressure over the North Atlantic, and "no blocking" includes any ensemble member that does not exhibit this dipole anomaly over Europe. The analysis in Figure 8 illustrates that the warm

anomaly over Europe is associated with low pressure in the North Atlantic, resulting in cyclonic activity, in concert with atmospheric blocking by high-pressure anticyclones over Northern Europe. As a result, the cold, polar air is blocked by the high pressure and brought to Central Europe and the Middle East, while the interface between high and low pressure over Western Europe results in anomalous southeasterly flow, bringing warmer continental air there, as was proposed by *Thordarson and Self* [2003]. The Laki simulations that exhibit this type of circulation (Figure 8a) show positive temperature anomalies over Western Europe, reaching above 3 K, most of which are significant at the 90% level (Figure 8b). On the other hand, the remaining Laki simulations do simulate low pressure and weak cyclonic activity over the North Atlantic, but do not simulate the high pressure over Northern Europe (Figure 8c). As a result, these simulations show the expected response to the volcanic eruption: significant cooling throughout Europe (Figure 8d). The noLaki simulations show similar patterns, where the ensemble members that simulate low pressure over the North Atlantic and high pressure over Northern Europe (Figure 8e) show warming that is similar to the warming in Figure 8b, though the anomalies in the noLaki ensemble reach further east, due to the absence of the eruption (Figure 8f). Finally, the noLaki simulations that do not exhibit this anomalous circulation (Figure 8g) also show significant warming (Figure 9h), but the warming is shifted north and east over Northern Europe and Scandinavia; this pattern is noticeably different from the warming in Figures 8b,f. Therefore, we conclude that the warm July of 1783 in Europe was an example of internal variability, and was not a consequence of the Laki eruption. Furthermore, Europe may have experienced even more extreme heat in the absence of the eruption.

The anomalous conditions in summer 1783 were not limited to Europe. In addition to the July heatwave, reports indicate that India, parts of China, and Egypt experienced severe drought in summer 1783 [*Volney*, 1788; *Wang and Zhao*, 1981; *Mooley and Pant*, 1981; *Xu*,

1988; *Pant et al.*, 1992]. Large reductions in precipitation are simulated in the Laki ensemble, with reductions in excess of −3 mm/day over the African Sahel and parts of India (Figure 9a). Precipitation reductions are also seen in China, though to a lesser extent. This reduction of the summer monsoon, as seen previously in response to tropical [*Zambri and Robock*, 2016] and high latitude eruptions [e.g., *Oman et al.*, 2005, 2006a], is consistent with a southward shift of the ITCZ, which is the expected response to the asymmetric cooling of the NH by aerosols injected at high latitudes [*Colose et al.*, 2016]. In Figures 9b-e, we also plot the zonal mean precipitation anomalies for the 4 seasons after the Laki eruption, as well as the ITCZ locations for the Laki and noLaki ensembles. We define the latitude of the ITCZ based on *Adam et al.* [2016]:

$$\phi_{max} = \frac{\int_{\phi_1}^{\phi_2} \phi [P \cos \phi]^N d\phi}{\int_{\phi_1}^{\phi_2} [P \cos \phi]^N d\phi},$$ (1)

where P is the area-weighted precipitation, $\phi_1 = 20°S$, $\phi_2 = 20°N$, and $N = 10$. Figure 9b shows only modest changes in the zonal mean precipitation during JJA 1783, with decreases at 10°N (the approximate latitude of the Sahel region) and 20°N, with a zonal-mean increase in precipitation between 10°N and the equator, with little shift in the ITCZ location based on Equation 1. As the seasons progress, the precipitation reduction at 10°N increases in magnitude, reaching below −1 mm/d in DJF 1783–1784 and MAM 1784. In addition, the increase in precipitation south of 10°N increases to just below 1 mm/d, while the location of the maximum increase shifts as far south as 5°S. In the three seasons after JJA 1783, there is a southward displacement of the ITCZ in response to the Laki eruption, though the shift is rather small.

3.3 Winter 1783–1784

In contrast to the warm summer of 1783, records show that winter 1783–1784 in Europe was cold and harsh [*Thordarson and Self*, 2003 and references therein; *Luterbacher et al.*, 2004; *D'Arrigo et al.*, 2011]. Benjamin Franklin wrote, "perhaps the winter of 1783–4,

was more severe, than any that had happened for many years" [*Franklin*, 1784]. *Thordarson and Self* [2003] wrote about historical accounts of "1-m thick snow" in April in the Jutland Peninsula.

Similarly to the anomalous summer, there is discussion as to whether the extremely cold winter of 1783–1784 was due to the Laki eruption, or just another example of climate variability. *D'Arrigo et al.* [2011] attributed the cold season to a combination of a negative phase of the NAO and a positive phase of ENSO. However, they argued the case that this coincidence of a negative NAO and positive ENSO was in fact random, and that there was no reason to believe that volcanic aerosols from the Laki eruption forced either of these phenomena. On the other hand, *Pausata et al.* [2015a, 2016] showed that high-latitude eruptions *can* increase the likelihood of an El Niño in the winter following the eruption. In addition, *Stothers* [1998] presented historical evidence of extremely cold winters in Europe in 934–935 and 939–940, related to the Eldgjá eruption in Iceland, the largest high-latitude eruption in the past 1100 years, suggesting that cold winters are a robust response to high-latitude eruptions.

Figure 10 shows the DJF 1783–1784 surface temperature anomalies for the reanalysis and the Laki ensemble. The EKF400 reanalysis shows significant cooling over parts of Europe and North America, though the anomalies are below 1 K in most places. On the other hand, the Laki ensemble (Figure 10b) shows extreme cooling over most of the NH continents, cooling which is not observed in the noLaki ensemble (not shown). The EKF400 reconstruction shows extreme cooling over most of Europe, and anomalies below –3 K covering a large area of Central Europe (Figure 11a). Western to Central Europe is the only NH landmass that does not see significant cooling in the Laki ensemble (Figure 11b). In contrast to the rest of the NH, the Laki and noLaki ensembles show similar mild conditions over Europe (Figure 11b–c).

The global temperature plots from the EKF400 reanalysis – which display very little change in most of the NH (Figures 4a and 10a) – may seem to be at odds with the model output, which shows significant cooling over much of the NH (Figures 4b and 10b). However, the sparse anomalies outside of Europe in winter and in low to mid latitudes in summer comes from a lack of input data. Specifically, for this period, most of the summer records come from tree ring records from boreal forests, while the winter records are limited to instrumental and written records in Europe [*Franke et al.*, 2017]. Thus, the areas without records are output from an ensemble of transient climate runs, and should not be expected to capture the forced variability of a volcanic eruption. To illustrate this, we plot in Figure 12 the difference in variability of the surface temperature field for the latter half of the 18th century with the 1951–2000 period of the Hadley Centre/Climatic Research Unit Temperature version 4 dataset [HadCRUT4; *Morice et al.*, 2012]. Figure 12a shows that, during this period, the EKF400 reanalysis captures the summertime climate variability best over Eurasia and northernmost North America, with variability in the tropics and midlatitudes underestimated by 75% or more in some regions compared to HadCRUT4. Similarly, for the winter (Figure 12b), the NH climate variability in EKF400 is closest to that of HadCRUT4 over Europe. The relatively low variability over Western Europe seen in Figure 12a indicates that the warming in July 1783 (Figure 5a) could even be underestimated in this reanalysis. On the other hand, the extreme cooling over Europe in DJF 1783–1784 appears to be a reliable estimate.

Figure 13 shows the sea level pressure anomalies for the September 1783–May 1784 for the difference between the Laki and noLaki ensembles. In September, the Laki ensemble shows a dipole-type response, with significant negative pressure over Western Hemisphere midlatitudes, and positive anomalies over the Eastern Hemisphere. While the winter average (DJF; not shown) does not show a negative NAO response, the monthly snapshots tell a

somewhat different story. Specifically, the North Atlantic region shows exhibits a +/–/+ tripole response in December, and positive pressure in January, though the January anomalies are only significant over a small part of Western Europe. On the other hand, in the late winter (FM) and even into April, a significant negative NAO-type response is simulated, with significant positive pressure at the pole and negative anomalies at midlatitudes. These anomalies are consistent with the negative tropospheric Arctic Oscillation (AO) pattern found in *Zambri et al.* [2018], which is manifested as an equatorward shift of the midlatitude tropospheric jet. Similarly to the sea-level pressure anomalies in Figure 13, the negative tropospheric AO anomaly is strongest in late winter and early spring.

In addition to the spatial patterns of sea level pressure anomalies, we quantified the NAO index by computing empirical orthogonal functions (EOFs) of the monthly sea level pressure anomalies north of 20°N and between 110°W and 70°E for each ensemble member. Each pressure data point is weighted by the square root of the grid area it represents, and the NAO index is defined as the principal component of the monthly anomalies of the sea level pressure projected onto the first EOF for the 25-year control run and normalized to unit variance. Figure 14 shows the NAO index for the mean of the Laki and noLaki ensembles and their differences. Similarly to Figure 13, in the fall and early winter the NAO indices for both ensembles, and therefore their difference, are close to 0. However, in February and March, the Laki mean NAO index is negative. The mean index for the Laki ensemble in April is slightly positive; however, the difference in mean index between the Laki and noLaki ensembles indicates a clear negative response in late winter/early spring, from February to April, in agreement with Figure 13.

The largest anomaly in the NAO time series presented in Figure 14 is a positive NAO in June 1783. This is based on our choice of initial conditions, a choice which was made based on synoptic conditions over Europe in June 1783, as well as ENSO initial conditions.

As a result, the four Junes chosen in which to initiate the Laki eruption happen to have a positive NAO phase. However, the spread in the rest of the NAO timeseries in both the Laki and noLaki ensembles do not indicate a bias based on this initial positive NAO condition.

We also analyzed the effect of the volcanic eruption on ENSO. To characterize ENSO in the simulations, we used monthly SST anomalies averaged over the Niño3.4 region (5°N to 5°S, 170°W to 120°W). We applied a 5-month running mean and divided the Laki and noLaki ensemble members into three groups according to the ENSO state that results in the winter following the eruption. We followed the convention of *Pausata et al.* [2016] in defining the ENSO state by the September 1783 through February 1784 average Niño3.4 index in the no-volcano control simulation: El Niño (Niño3.4 index > 0.6 K), La Niña (Niño3.4 index < –0.6 K), and neutral (–0.6 K < Niño3.4 index < 0.6 K) case. Figure 15 shows the Niño 3.4 indices for the two ensembles for the year after the Laki eruption. In all three cases (La Niña, neutral, and El Niño incipient state), the Laki ensemble simulates a significantly positive anomaly in the ENSO state when compared with the noLaki ensemble. This result is in agreement with *Pausata et al.* [2016], who found that the southward-shifted ITCZ after a high-latitude volcanic eruption leads to a positive ENSO anomaly.

4. Summary and Discussion

We have conducted an ensemble of model simulations of the 1783–1784 Laki volcanic eruption in Iceland to analyze its effect on regional and Northern Hemisphere climate in the year following the eruption. Results indicate that the abnormally warm summer in Europe in 1783 was in fact due to the internal variability of the climate system. Specifically, atmospheric blocking as a result of anomalously high pressure over Northern Europe caused the cold polar air to bypass Western Europe to Central Europe and the Middle East, and Europe may have been even warmer had the eruption not occurred. Though *Thordarson and Self* [2003] correctly proposed the persistence of southerly weather as the

cause of the warmth, this is the first modeling study to simulate the warm European July in conjunction with the Laki eruption. The main conclusion of the study of the summer of 1783 is that this unusual anomaly should not be expected after a future Laki-type eruption, and that the expected climate response is, in fact, cooling.

We find a robust decrease in tropical precipitation in the summer of 1783, specifically over the Sahel region of Africa, as a result of the southward shift of the ITCZ from the asymmetric cooling of the NH. This is consistent with reports of low Nile River flow, drought and famine in Egypt after the Laki eruption, and the results are in agreement with similar modeling studies [*Oman et al.*, 2006a; *Colose et al.*, 2016; *Manning et al.*, 2017]. Precipitation anomalies are less homogeneous, exhibiting significant wetting in the south, and drying in the north.

It has been hypothesized that the anomalously cold winter in 1783–1784 was caused by a negative phase of the NAO in combination with a positive phase of ENSO [*D'Arrigo et al.*, 2011]. We find no dynamic circulation response to the eruption that indicates Laki caused a negative NAO in the traditionally defined "DJF" winter. However, in looking at monthly anomalies, we do find a robust negative NAO response in late winter and early spring, specifically in February to April 1784. In addition, we find a robust ENSO response to a positive ENSO phase as a result of the Laki eruption, in agreement with *Pausata et al.* [2015a, 2016].

We used the best available Laki SO_2 emissions budget – that constructed by *Thordarson et al.* [1996]. However, even the best estimate includes uncertainties, which past studies have estimated to be about $\pm20\%$ [*Stevenson et al.*, 2003; *Oman et al.*, 2006b]. In addition to the uncertainties in the amount of SO_2 released by the Laki eruption, there are uncertainties with regard to the injection height of the gas. Different injection heights would affect the proportion of gas that reaches the stratosphere or stays in the troposphere. This

would have a significant effect on both the climate responses analyzed here and the atmospheric composition and circulation responses analyzed in *Zambri et al.* [2018]. Future work will explore these uncertainties by varying the injection height as well as the amount of SO_2 injected. The results presented in this study are important not only for historical purposes, but also for predicting the climate response to future Icelandic flood lava eruptions.

References

Adam, O., T. Bischoff, and T. Schneider (2016), Seasonal and interannual variations of the energy flux equator and ITCZ. part I: zonally averaged ITCZ position, *J. Clim.*, *29*, doi: 10.1175/JCLI-D-15-0512.1.

Bentsen, M., et al. (2013), The Norwegian Earth System Model, NorESM1-M part 1: description and basic evaluation of the physical climate, *Geosci. Model Dev.*, *6*(3), 687–720. doi: 10.5194/gmd-6-687-2013.

Bittner, M., H. Schmidt, C. Timmreck, and F. Sienz (2016a), Using a large ensemble of simulations to assess the Northern Hemisphere stratospheric dynamical response to tropical volcanic eruptions and its uncertainty, *Geophys. Res. Lett.*, *43*, 9324–9332, doi:10.1002/ 2016GL070587.

Bittner, M., C. Timmreck, H. Schmidt, M. Toohey, and K. Krüger (2016b), The impact of wave-mean flow interaction on the Northern Hemisphere polar vortex after tropical volcanic eruptions, *J. Geophys. Res. Atmos.*, *121*, 5281–5297, doi:10.1002/2015JD024603.

Butchart, N. (2014), The Brewer-Dobson circulation, *Rev. Geophys.*, *52*, 157–184, doi:10.1002/2013RG000448.

Cassou, C. and J. Cattiaux (2016), Disruption of the European climate seasonal clock in a warming world, *Nature Climate Change*, *6*, 589–594, doi:10.1038/nclimate2969.

Christiansen, B. (2008), Volcanic eruptions, large-scale modes in the Northern Hemisphere, and the El Niño–Southern Oscillation, *J. Clim.*, *21*, 910–922.

Colose, C. M., A. N. LeGrande, and M. Vuille (2016), Hemispherically asymmetric volcanic forcing of tropical hydroclimate during the last millennium, *Earth Syst. Dyn.*, *7*, 681-696, doi:10.5194/esd-7-681-2016.

Cook, E. and P. Krusic (2004), North American Drought Atlas. *NOAA Paleoclimatol.*, Boulder, CO.

D'Arrigo, R., R. Seager, J. E. Smerdon, A. N. LeGrande, and E. R. Cook (2011), The anomalous winter of 1783–1784: Was the Laki eruption or an analog of the 2009–2010 winter to blame?, *Geophys. Res. Lett.*, *38*, L05706, doi:10.1029/2011GL046696.

de Lamanon, R. P. C. (1799), Observations on the nature of the fog of 1783, *A. Tilloch's Phil. Mag. London*, 80–89.

de Montredon, M. M. (1784), Recherches sur l'origin & sur la nature des Vapeurs qui ont re´gne´ dans l'Atmosphe`re pendant l'e´te´ de 1783, *Mem. Acad. R. Sci., Paris*, MDCCLXXXI, 754–773.

Durand, M., and J. Grattan (1999), Extensive respiratory health effects of volcanogenic dry fog in 1783 inferred from European documentary sources, *Environ. Geochem. Health*, *21*, 371–376.

Franke, J., S. Brönnimann, J. Bhend, and Y. Brugnara (2017), A monthly global paleo-reanalysis of the atmosphere from 1600 to 2005 for studying past climatic variations, *Scientific Data*, *4*, 170076, doi:10.1038/sdata.2017.76.

Franklin, B. (1784), Meteorological imaginations and conjectures, *Manchester Lit. Philos. Soc. Mem. Proc.*, *2*, 122.

Gettelman, A., X. Liu, S. J. Ghan, H. Morrison, S. Park, A. J. Conley, S. A. Klein, J. Boyle, D. L. Mitchell, and J. L. F. Li (2010), Global simulations of ice nucleation and ice supersaturation with an improved cloud scheme in the Community Atmosphere Model, *J. Geophys. Res.*, *115*, D18216, doi:10.1029/2009JD013797.

Grattan J., M. Durand, and S. Taylor (2003), Illness and elevated human mortality in Europe coincident with the Laki fissure eruption. *Volcanic Degassing*, eds C. Oppenheimer, D.

M. Pyle, and J .Barclay (Geological Soc, London), Special Publications, *213*, pp. 401–414.

Grattan, J. P., and J. Sadler (1999), Regional warming of the lower atmosphere in wake of volcanic eruptions: The role of the Laki fissure eruption in the hot summer of 1783, *Geol. Soc. London*, Spec. Publ., *16*, 161–172.

Hamilton, W. (1783), An account of the earthquakes which happened in Italy from February to May 1783, part 1, *Philos. Trans. R. Soc. London*, LXXII, 169–208.

Hantemirov, R. M., L. A. Gorlanova, and S. G. Shiyatov (2004), Extreme temperature events in summer in northwest Siberia since AD 742 inferred from tree rings, *Palaeogeogr. Palaeoclimatol. Palaeoecol.*, *209*(1–4), 155–164, doi:10.1016/j.palaeo.2003.12.023.

Highwood, E. J., and D. S. Stevenson (2003), Atmospheric impact of the 1783–1784 Laki Eruption: Part II Climatic effect of sulphate aerosol, *Atmos. Chem. Phys.*, *3*(4), 1177–1189, doi: 10.5194/acp-3-1177-2003.

Hólm, S. M. (1784), *About the Earth Fire in Iceland in the Year 1783*, 83 pp., Peder Horrebow, Copenhagen.

Hurrell, J. W. (1995), Decadal trends in the North Atlantic Oscillation: Regional temperatures and precipitation, *Science*, *269*, 676–679.

Hurrell, J. W., et al. (2013), The community earth system model: A framework for collaborative research, *Bull. Am. Meteorol. Soc.*, *94*, 1339–1360, doi:10.1175/BAMS-D-12-00121.1.

Jacoby, G. C., K. W. Workman, and R. D. D'Arrigo (1999), Laki eruption of 1783, tree rings, and disaster for northwest Alaska Inuit, *Quat. Sci. Rev.*, *18*(12), 1365–1371, doi:10.1016/S0277-3791(98)00112-7.

Jones, A. C., J. M. Haywood, N. Dunstone, K. Emanuel, M. K. Hawcroft, K. I. Hodges, and A. Jones (2017), Impacts of hemispheric solar geoengineering on tropical cyclone frequency, *Nature Communications*, *8*, 1382, doi:10.1038/s41467-017-01606-0.

Kay, J. E., et al. (2015), The Community Earth System Model (CESM) Large Ensemble Project: A Community Resource for Studying Climate Change in the Presence of Internal Climate Variability, *Bull. Am. Meteorol. Soc.*, *96*, 1333–1349, doi: 10.1175/BAMS-D-13-00255.1.

Kington, J. A. (1978), Historical daily synoptic weather maps from the 1780's, *J. Meteorol.*, *3*, 65–70.

Kington, J. A. (1988), *The Weather of the 1780's Over Europe*, 164 pp., Cambridge Univ. Press, New York.

Kodera, K., M. Chiba, K. Yamazaki, and K. Shibata (1991), A possible influence of the polar night stratospheric jet on the subtropical tropospheric jet, *J. Meteorol. Soc. Jpn.*, *69*(6), 715–721.

Kravitz, B., and A. Robock (2011), Climate effects of high-latitude volcanic eruptions: Role of the time of year, *J. Geophys. Res.*, *116*, D01105, doi:10.1029/2010JD014448.

Liu, X., et al. (2012), Toward a minimal representation of aerosols in climate models: Description and evaluation in the Community Atmosphere Model CAM5, *Geosci. Model Dev.*, *5*(3), 709–739, doi:10.5194/gmd-5-709-2012.

Luterbacher, J., Dietrich, D., Xoplaki, E., Grosjean, M., and Wanner, H. (2004), European seasonal and annual temperature variability, trends, and extremes since 1500, *Science*, *303*, 1499–1503.

Malavelle, et al. (2017), Strong constraints on aerosol-cloud interactions from volcanic eruptions, *Nature*, *546*, 485–491, doi:10.1038/nature22974.

Manley, G. (1974), Central England temperatures: Monthly means 1659 –1973, *Q. J. R. Meteorol. Soc.*, *100*, 389–405.

Marsh, D., M. Mills, D. E. Kinnison, and J. -F. Lamarque (2013), Climate change from 1850 to 2005 simulated in CESM1(WACCM), *J. Clim.*, *26*, 7372–7391, doi:10.1175/JCLI-D-12-00558.1.

Marshall, A. G., A. A. Scaife, and S. Ineson (2009), Enhanced seasonal prediction of European winter warming following volcanic eruptions, *J. Clim.*, *22*(23), 6168–6180, doi:10.1175/2009JCLI3145.1.

Mills, M. J., et al. (2016), Global volcanic aerosol properties derived from emissions, 1990–2014, using CESM1(WACCM), *J. Geophys. Res. Atmos.*, *121*, 2332–2348, doi:10.1002/2015JD024290.

Mills, M. J. et al. (2017), Radiative and chemical response to interactive stratospheric sulfate aerosols in fully coupled CESM1(WACCM), *J. Geophys. Res. Atmos.*, *122*(23), 13,061–13,078, doi:10.1002/2017JD027006.

Mooley, D. A., and G. B. Pant (1981), *Droughts in India over the last 200 years, their socio-economic impacts and remedial measures for them, in Climate and History: Studies in Past Climates and Their Impact on Man*, edited by T. M. L. Wigley, M. J. Ingram, and G. Farmer, pp. 465–478, Cambridge Univ. Press, New York.

Morice, C. P., J. J. Kennedy, N. A. Rayner, and P. D. Jones, (2012), Quantifying uncertainties in global and regional temperature change using an ensemble of observational estimates: the HadCRUT4 dataset, *J. Geophys. Res.*, *117*, D08101, doi:10.1029/2011JD017187.

Morrison, H., and A. Gettelman (2008), A new two-moment bulk stratiform cloud microphysics scheme in the Community Atmosphere Model, Version 3 (CAM3). Part I: Description and numerical tests, *J. Clim.*, *21*, 3642, doi:10.1175/2008JCLI2105.1.

Oman, L., A. Robock, G. Stenchikov, G. A. Schmidt, and R. Ruedy (2005), Climatic response to high-latitude volcanic eruptions, *J. Geophys. Res.*, *110*, D13103, doi:10.1029/2004JD005487.

Oman, Luke, A. Robock, G. L. Stenchikov, and T. Thordarson (2006a), High-latitude eruptions cast shadow over the African monsoon and the flow of the Nile, *Geophys. Res. Lett.*, *33*, L18711, doi:10.1029/2006GL027665.

Oman, L., A. Robock, G. L. Stenchikov, T. Thordarson, D. Koch, D. T. Shindell, and C. Gao (2006b), Modeling the distribution of the volcanic aerosol cloud from the 1783–1784 Laki eruption, *J. Geophys. Res.*, *111*, D12209, doi:10.1029/2005JD006899.

Pant, G. B., B. Parthasarathy, and N. A. Sontakke (1992), *Climate over India during the first quarter of the nineteenth century, in The Year Without a Summer?*, edited by C. R. Harrington, pp. 429–435, Can. Mus. of Nature, Ottawa.

Parker, D. E., T. P. Legg, and C. K. Folland (1992), A new daily Central England Temperature series, 1772–1991, *Int. J. Climatol.*, *12*, 317–342.

Pausata, F. S. R., Chafik, L., Caballero, R., Battisti, D. S. (2015a), Impacts of a high-latitude volcanic eruption on ENSO and AMOC, *Proc. Natl. Acad. Sci.*, *112*(45), 13784–13788.

Pausata, F. S. R., A. Grini, R. Caballero, A. Hannachi and Ø. Seland (2015b), High-latitude volcanic eruptions in the Norwegian Earth System Model: the effect of different initial conditions and of the ensemble size, *Tellus B: Chemical and Physical Meteorology*, *67*:1, 26728, DOI: 10.3402/tellusb.v67.26728.

Pausata, F.S.R, Karamperidou, C., Caballero, R., and Battisti, D.S. (2016), ENSO response to high-latitude volcanic eruptions in the Northern Hemisphere: the role of the initial conditions, *Geophys. Res. Lett.*, *43*(16), 8694–8702.

Perlwitz, J., and H. –F. Graf (1995), The statistical connection between tropospheric and stratospheric circulation of the Northern Hemisphere in winter, *J. Clim.*, *8*, 2282–2295.

Rampino, M. R., T. Thordarson, and S. Self (1999), A new volcanism/climate connection: Tropospheric SO_2 greenhouse effect from the Laki (Iceland) 1783 fissure eruption, in IUGG XXI General Assembly, p. 278.

Robock, A., and J. Mao (1995), The volcanic signal in surface temperature observations, *J. Clim.*, *8*, 1086–1103.

Robock, Alan (2000), Volcanic eruptions and climate, *Rev. Geophys.*, *38*, 191-219.

Schmidt, A., et al. (2018), Volcanic radiative forcing from 1979 to 2015, *J. Geophys. Res.: Atmos.*, *123*, doi:10.1029/2018JD028776.

Schmidt, A., K. S. Carslaw, G. W. Mann, M. Wilson, T. J. Breider, S. J. Pickering, and T. Thordarson (2010), The impact of the 1783-1784 AD Laki eruption on global aerosol formation processes and cloud condensation nuclei, *Atmos. Chem. Phys.*, *10*(13), 6025–6041, doi:10.5194/acp-10-6025-2010.

Schmidt, A., B. Ostro, K.S. Carslaw, M. Wilson, T. Thordarson, G.W. Mann, and A.J. Simmons (2011), Excess mortality in Europe following a future Laki-style Icelandic eruption, *Proc. Nat. Acad. Sci.*, *108*(38), 15710–15715, doi:10.1073/pnas.1108569108.

Schmidt, A., T. Thordarson, L. D. Oman, A. Robock (2012), and S. Self, Climatic impact of the long-lasting 1783 Laki eruption: inapplicability of mass-independent sulfur isotopic composition measurements, *J. Geophys. Res.*, *117*, D23116, doi:10. 1029/2012JD018414.

Schmidt, G. A., et al. (2006), Present day atmospheric simulations using GISS ModelE: comparison to in situ, satellite, and reanalysis data, *J. Clim.*, *19*, doi: 10.1175/JCLI3612.1.

Schneider, D. P., C. M. Ammann, B. L. Otto-Bliesner, and D. S. Kaufman (2009), Climate response to large, high-latitude and low-latitude volcanic eruptions in the Community Climate System Model, *J. Geophys. Res.*, *114*, D15101, doi:10.1029/2008JD011222.

Stevenson, D. S., C. E. Johnson, E. J. Highwood, V. Gauci, W. J. Collins, and R. G. Derwent (2003), Atmospheric impact of the 1783–1784 Laki eruption: Part I Chemistry modelling, *Atmos. Chem. Phys.*, *3*(3), 487–507, doi:10.5194/acp-3-487-2003.

Stothers, R. B. (1998), Far reach of the tenth century Eldgjá eruption, Iceland, *Climatic Change*, *39*(4), 715–726.

Stott, P. A., D. A. Stone, and M. R. Allen (2004), Human contribution to the European heatwave of 2003, *Nature*, *432*, 610–614.

Thompson, D. W. J., and J. M. Wallace (1998), The Arctic Oscillation signature in the wintertime geopotential height and temperature fields, *Geophys. Res. Lett.*, *25*, 1297–1300, doi:10.1029/98GL00950.

Thordarson, T., and S. Self (1993), The Laki (Skaftar Fires) and Grimsvötn eruptions in 1783–1785, *Bull. Volcanol.*, *55*(4), 233-263.

Thordarson, T., and S. Self (2003), Atmospheric and environmental effects of the 1783–1784 Laki eruption: A review and reassessment, *J. Geophys. Res.*, *108*(D1), 4011, doi:10.1029/2001JD002042.

Thordarson, T., S. Self, D. J. Miller, G. Larsen, and E. G. Vilmundardóttir (2003), Sulphur release from flood lava eruptions in the Veidivötn, Grímsvötn and Katla volcanic systems, Iceland, *Geological Society, London, Special Publications*, *213*(1), 103–121.

Thordarson, T., S. Self, N. Oskarsson, and T. Hulsebosch (1996), Sulfur, chlorine, and fluorine degassing and atmospheric loading by the 1783-1784 AD Laki (Skaftar fires) eruption in Iceland, *Bull. Volcanol.*, *58*(2-3), 205-222.

Timmreck, C. (2012), Modeling the climatic effects of large explosive volcanic eruptions, *Wiley Interdiscip. Rev. Clim. Change*, *3*, 545–564, doi:10.1002/wcc.192.

van Loon, H. and J. C. Rogers (1783), The seesaw in winter temperatures between Greenland and Northern Europe. Part I: general description, *Mon. Weath. Rev.*, *106*, 296–310.

van Swinden, S. P. (1783), Observations on the cloud which appeared in June 1783, in *Emphemerides Societatis Meteorologicae Palatinae, Observationes Anni 1783*, edited by J. Hemmer and C. König, pp. 679–688, Fr. Scwan, Mannheim, Germany.

Vehkamäki, H., M. Kulmala, I. Napari, K. Lehtinen, C. Timmreck, M. Noppel, and A. Laaksonen (2002), An improved parameterization for sulfuric acid-water nucleation rates for tropospheric and stratospheric conditions, *J. Geophys. Res.*, *107*(D22), 4622, doi:10.1029/2002JD002184.

Volney, M. C. -F. (1788), *Travels Through Syria and Egypt, in the Years 1783, 1784, and 1785*, vol. 1, 258 pp., Burnet, White, Byrne, W. Porter, Moore and Dornin, Dublin.

Wang, S.-W., and Z.-C. Zhao (1981), *Droughts and floods in China, 1470–1979, in Climate and History: Studies in Past Climates and Their Impact on Man*, edited by T. M. L. Wigley, M. J. Ingram, and G. Farmer, pp. 271–288, Cambridge Univ. Press, New York.

Witham C. S., and C. Oppenheimer (2004), Mortality in England during the 1783–1784 Laki craters eruption, *Bull. Volcanol.*, 67, 15–26.

Wood, C. A. (1992), *Climatic effects of the 1783 Laki eruption, in The Year Without a Summer?*, edited by C. R. Harington, pp. 58–77, Can. Mus. of Nature, Ottawa.

White, G. (1789), *The Natural History of Selborne*, 296 pp., Cresset Press, London.

White, G. (1970), *Gilberts White's Journals, 1768–1793*, 463 pp., David & Charles Reprints, Great Britain.

Xu, Q. (1988), *The abnormally cold summers of central China and their relation to volcanic eruptions, in Aerosols and Climate*, edited by P. V. Hobbs and M. McCormick, pp. 223–231, A. Deepak, Hampton, Va.

Zambri, B., A. N. LeGrande, A. Robock, and Joanna Slawinska (2017), Northern Hemisphere winter warming and summer monsoon reduction after volcanic eruptions over the last millennium, *J. Geophys. Res. Atmos.*, *122*, doi:10.1002/2017JD026728.

Zambri, B., and A. Robock (2016), Winter warming and summer monsoon reduction after volcanic eruptions in Coupled Model Intercomparison Project 5 (CMIP5) simulations, *Geophys. Res. Lett.*, *43*, 10,920-10,928, doi:10.1002/2016GL070460.

Zambri, B., A. Robock, M. J. Mills, and A. Schmidt (2018), Modeling the 1783–1784 Laki eruption in Iceland, part I: Aerosol evolution and global stratospheric circulation impacts, submitted to *J. Geophys. Res. Atmos.*

Table 1. Dates of stratospheric eruptions and SO_2 emissions for the ten stratospheric eruption episodes from the Laki eruption [*Thordarson and Self*, 2003].

Date (1783)	Stratospheric SO_2 (Tg)
June 8	8.3
June 11	13.5
June 14	18.7
June 27	10.8
July 9	8.9
July 29	13.2
August 31	7.7
September 9	5.9
September 26	4.4
October 25	2.9

Table 2. Surface emissions of SO_2 for each month of the Laki eruption [*Thordarson and Self*, 2003].

Month	Surface SO_2 (Tg)
June 1783	10.19
July 1783	4.54
August 1783	3.25
September 1783	3.31
October 1783	1.22
November 1783	2.69
December 1783	1.44
January 1784	0.79
February 1784	0.13
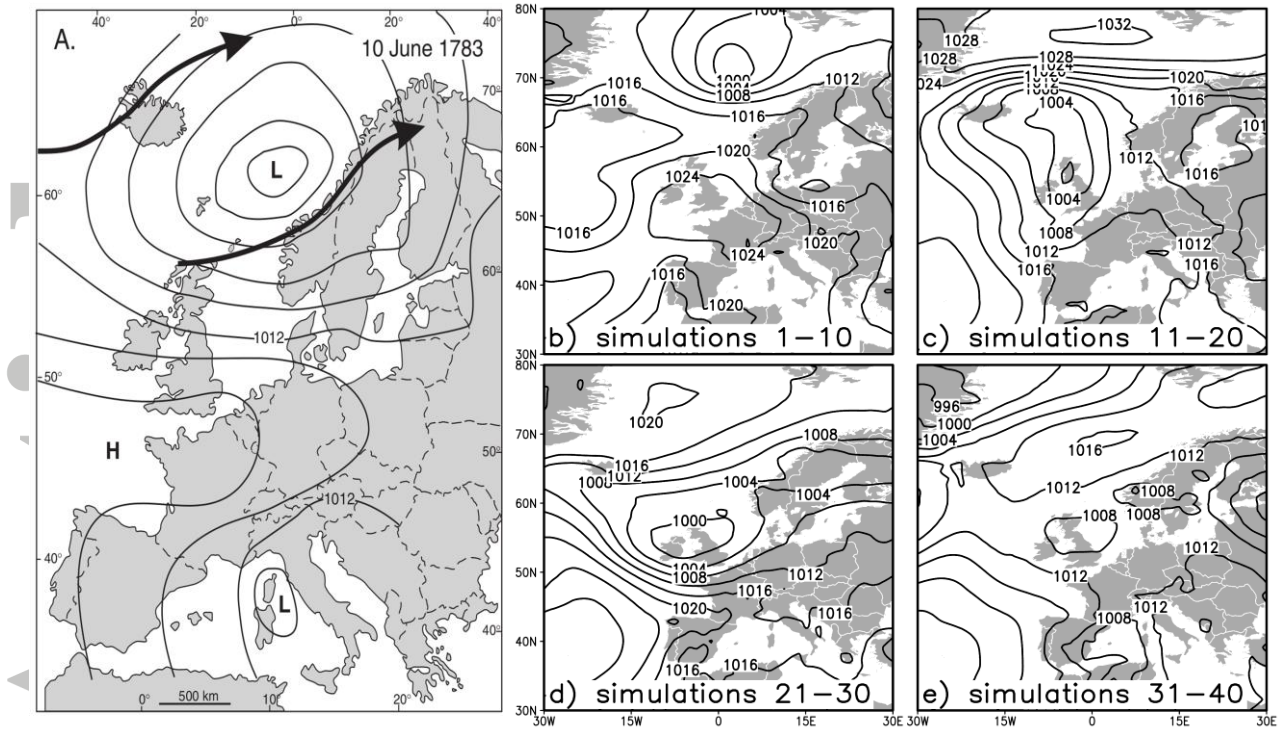
Figure 1. Sea level pressure (hPa) maps for: (a) 8–12 June 1783 drawn from *Kington* [1988] [Figure 6a, *Thordarson and Self*, 2003]; contours at 4 hPa intervals) and (b)-(e) 8 June 1783 from initial conditions for the CESM1(WACCM) simulations, showing the circulation patterns over Europe.
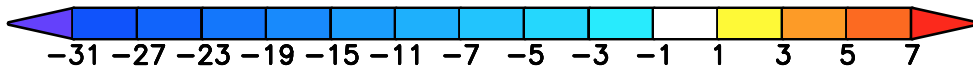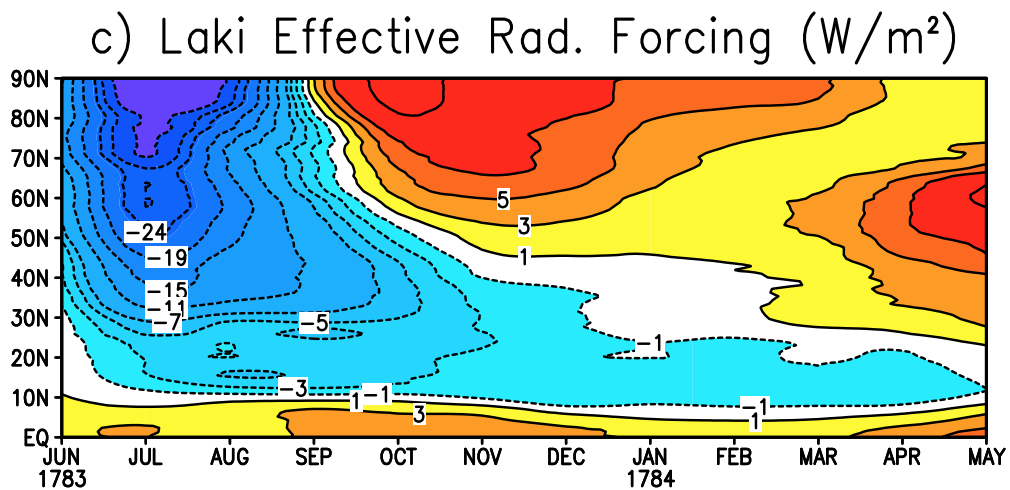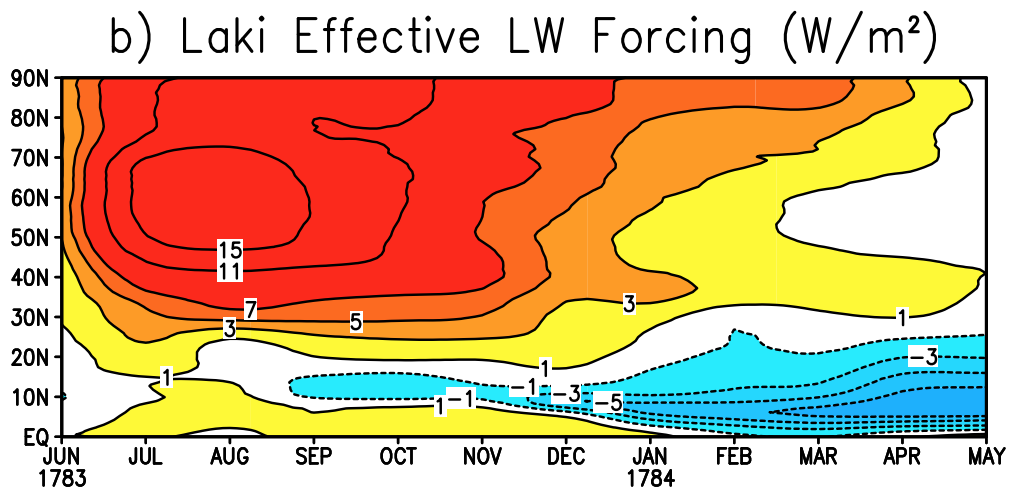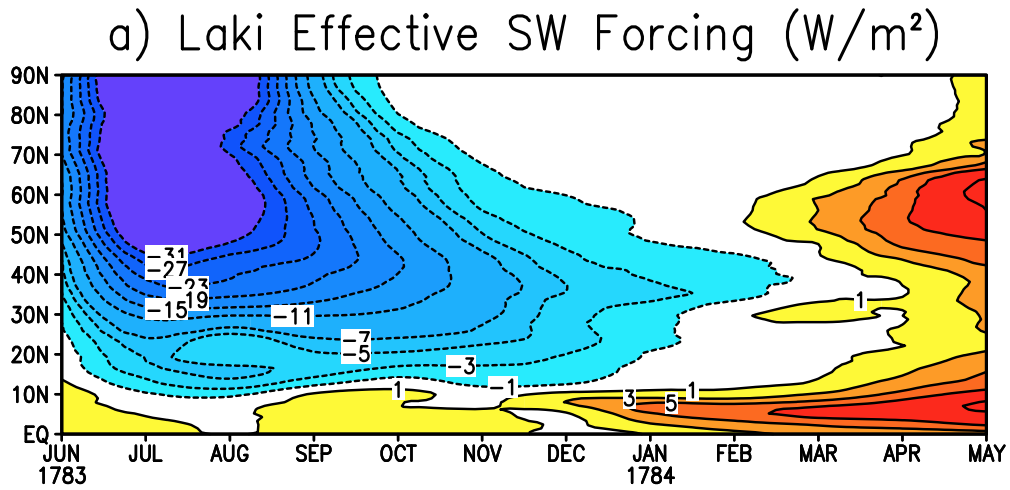
Figure 2. Zonal-average Northern Hemisphere effective radiative forcing (W/m², positive downward) for the average of 40 model simulations with the Laki eruption for (a) shortwave, (b) longwave, and (c) net shortwave plus longwave.

(a) NH TOA Residual Energy Balance

(b) NH Temperature Anomaly
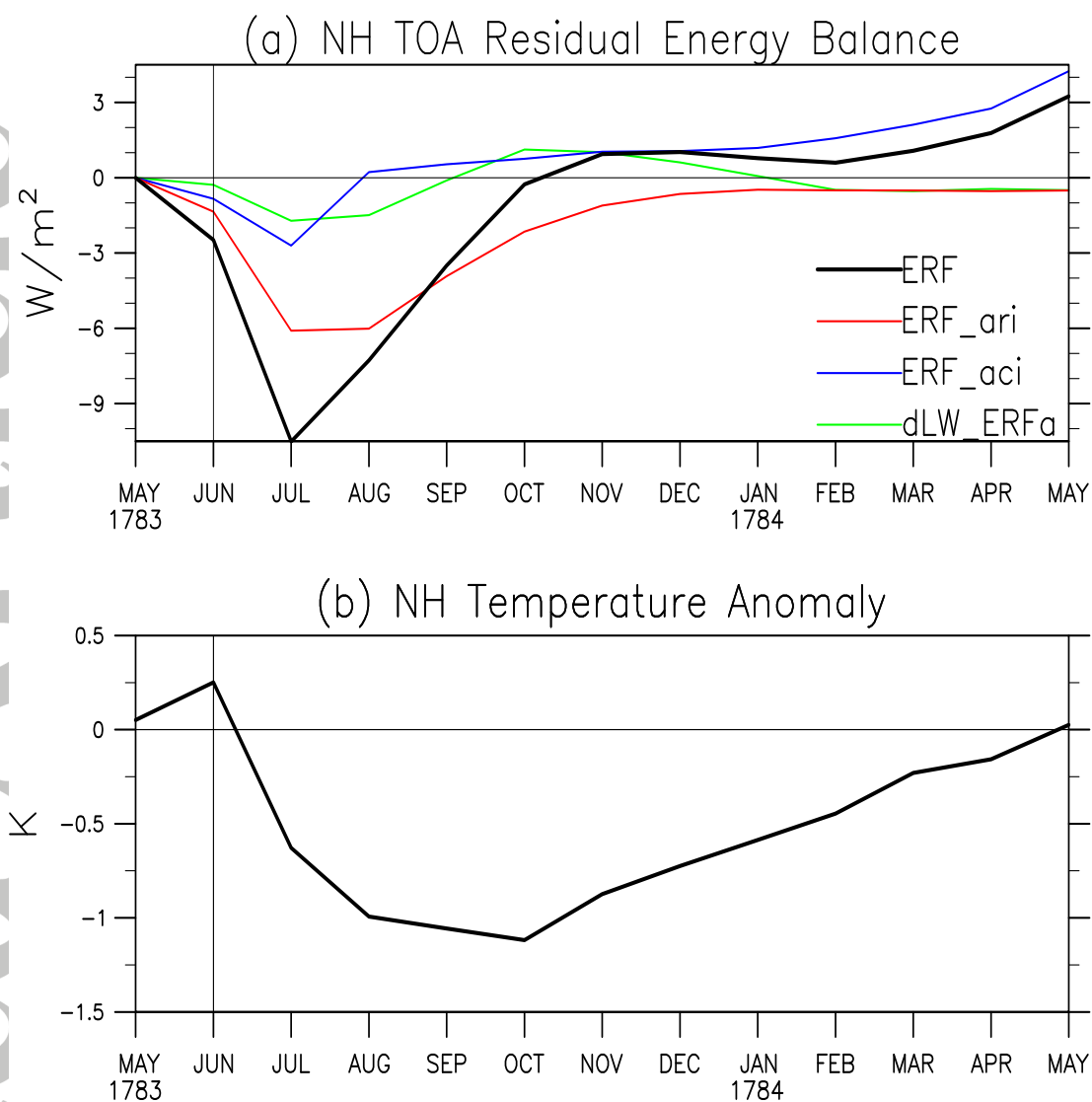
Figure 3. (a) Time series of ensemble mean NH total volcanic effective radiative forcing (ERF, in Wm^{-2}, black line). The volcanic ERF is decomposed into the forcings from aerosol-radiation interactions (ERFari, red line), aerosol-cloud interactions (ERFaci, blue line), and a longwave atmosphere adjustment and surface albedo term (dLW_ERFa, green line). (b) Time series of ensemble mean NH-average surface air temperature change. Shading indicates one standard deviation of the monthly mean anomaly.
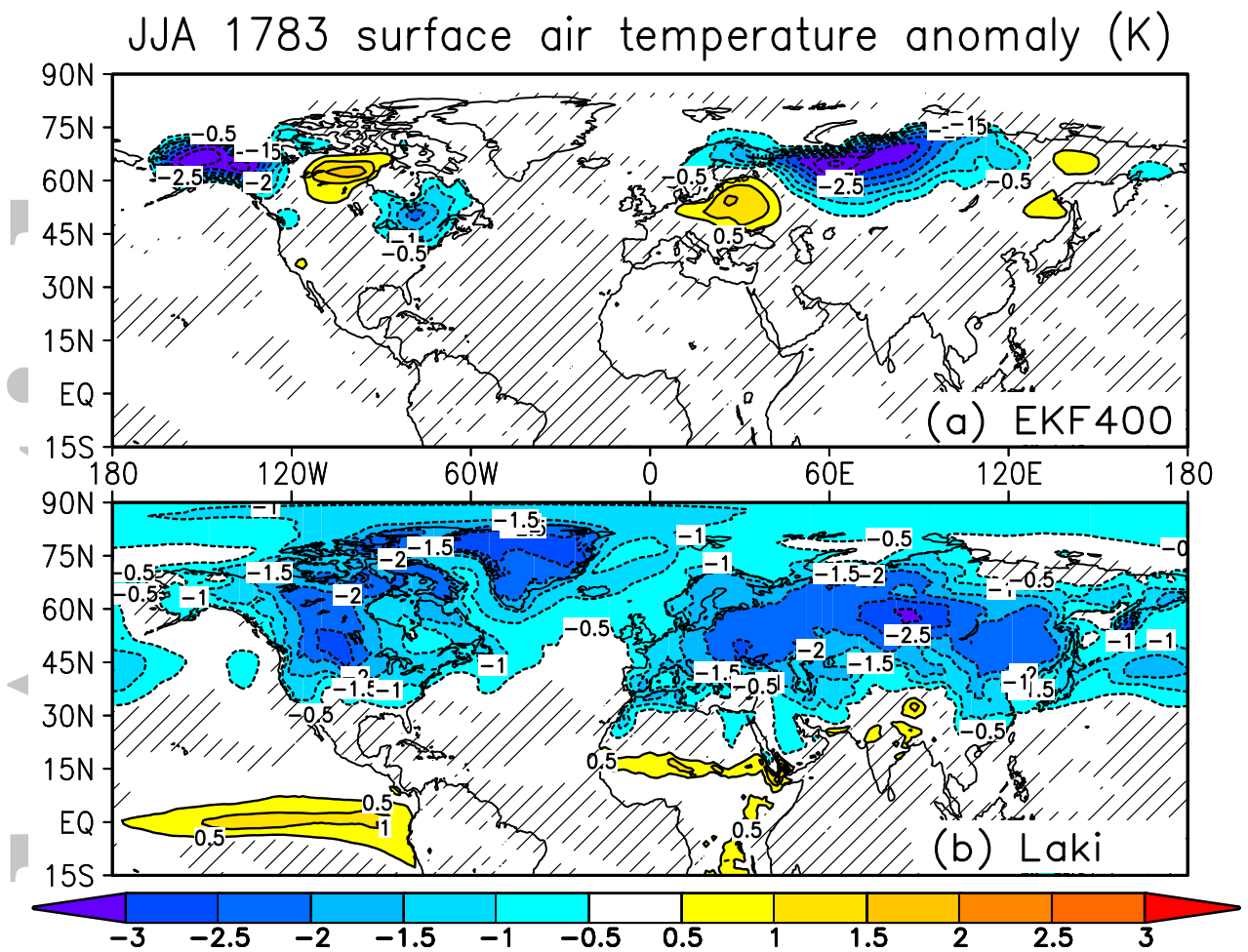
Figure 4. JJA 1783 surface air temperature anomalies (K) for (a) EKF400 reanalysis [*Franke et al.*, 2017] and (b) average of Laki ensemble. Anomalies are calculated with respect to the five years before the eruption. Hatching represents areas < 95% significance using a two-tailed Student's *t*-test.
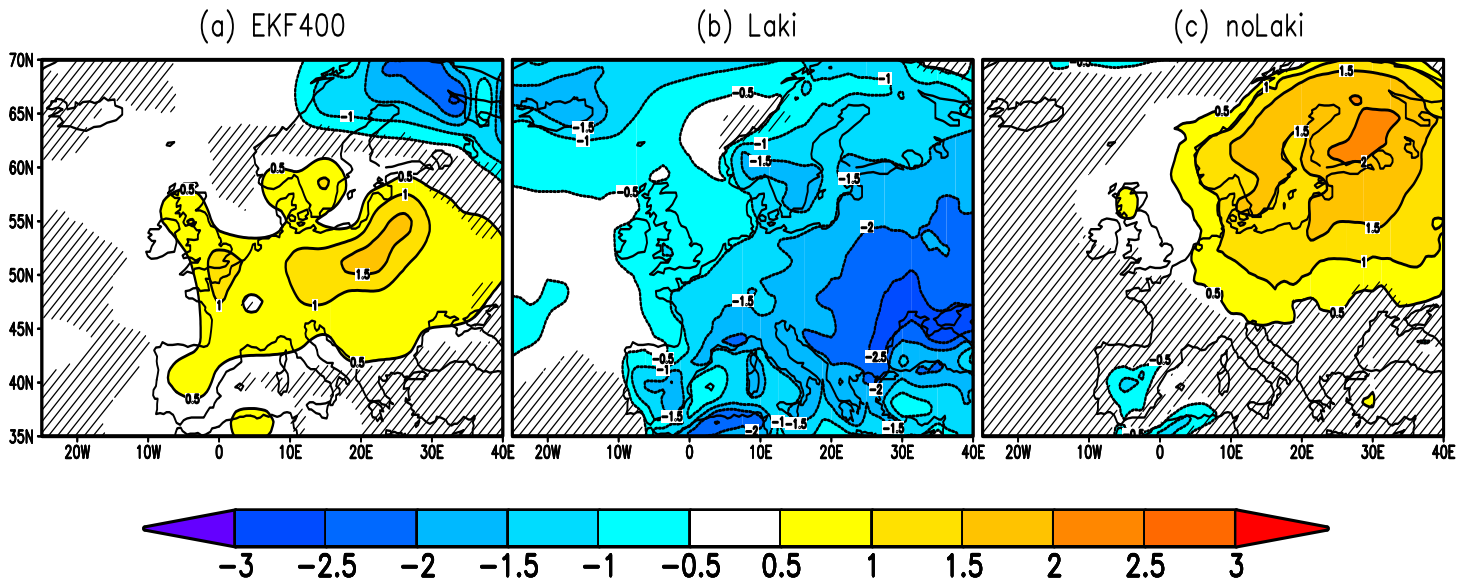
Figure 5. July 1783 European surface temperature anomalies (K) for (a) EKF400 reanalysis [*Franke et al.*, 2017], (b) Laki ensemble average, and (c) noLaki ensemble average. Anomalies are calculated with respect to the five years before the eruption. Hatching represents areas < 95% significance using a two-tailed Student's *t*-test.
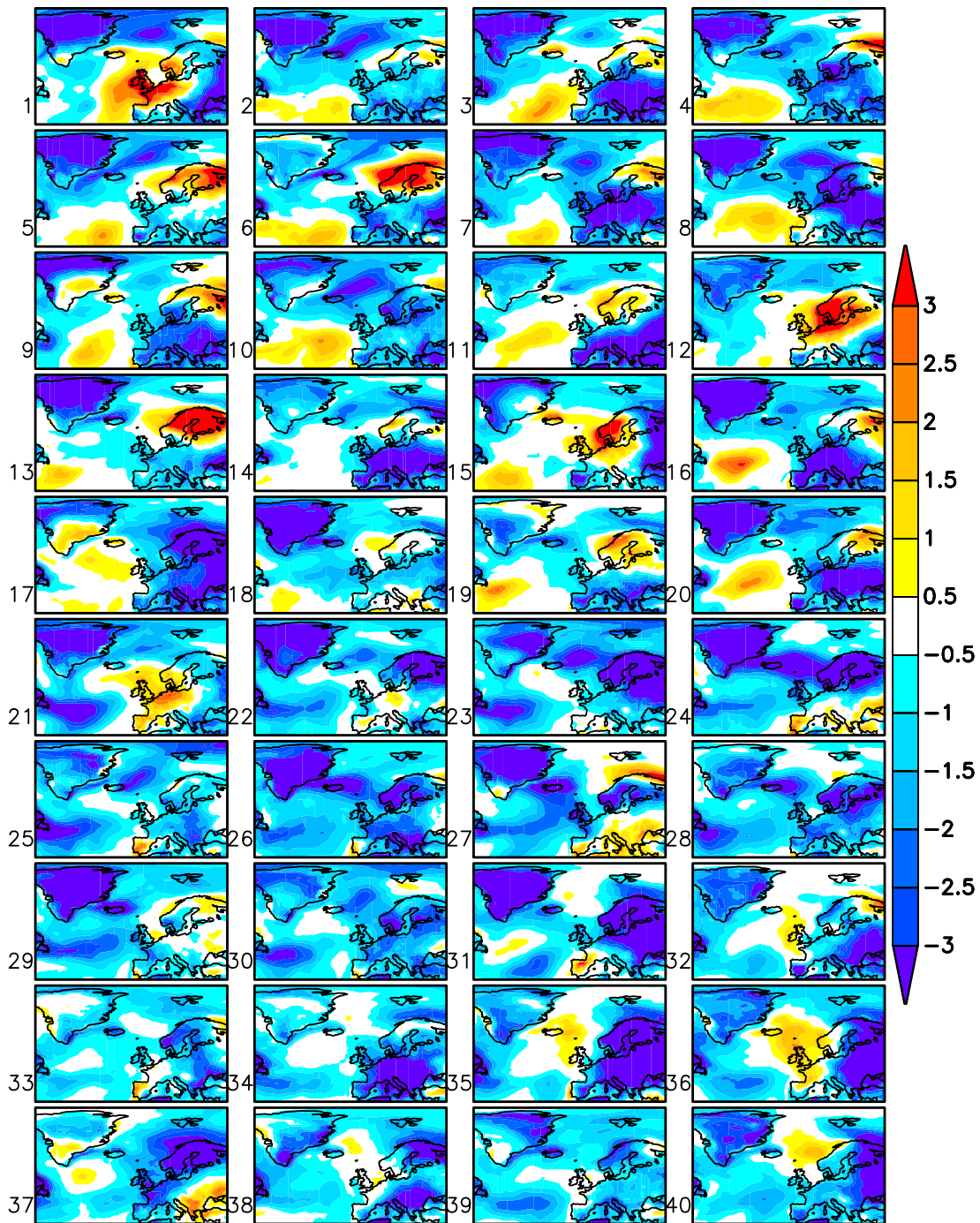
Figure 6. July 1783 European surface temperature anomalies (K) for individual Laki simulations. Anomalies are calculated with respect to the five years before the eruption. Simulations 1–10 were initialized from Figure 1b, 11–20 from Figure 1c, 21–30 from Figure 1d, and 31–40 from Figure 1d.
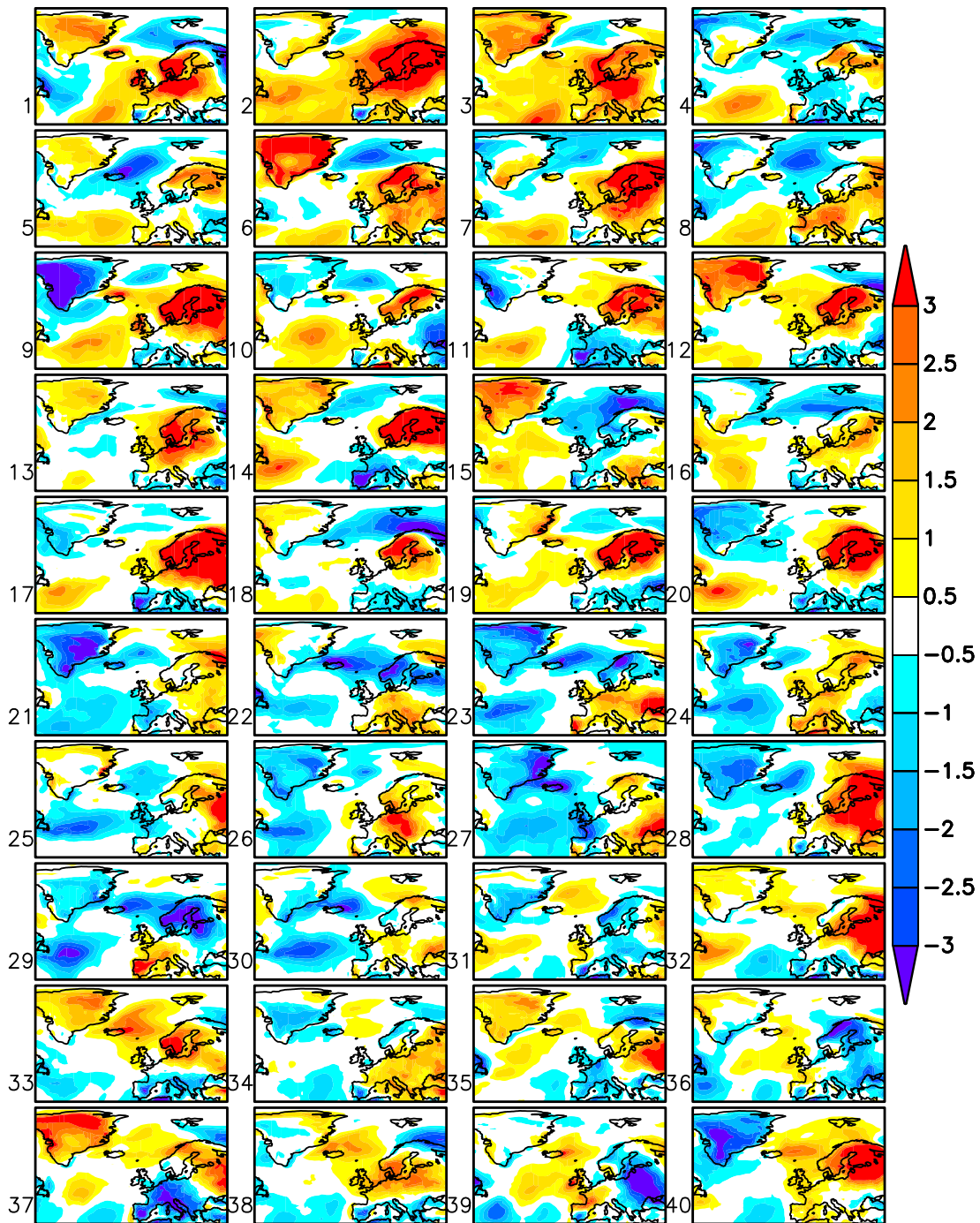
Figure 7. July 1783 European surface temperature anomalies (K) for individual noLaki simulations. Anomalies are calculated with respect to the five years before the eruption. Simulations 1–10 were initialized from Figure 1b, 11–20 from Figure 1c, 21–30 from Figure 1d, and 31–40 from Figure 1d.
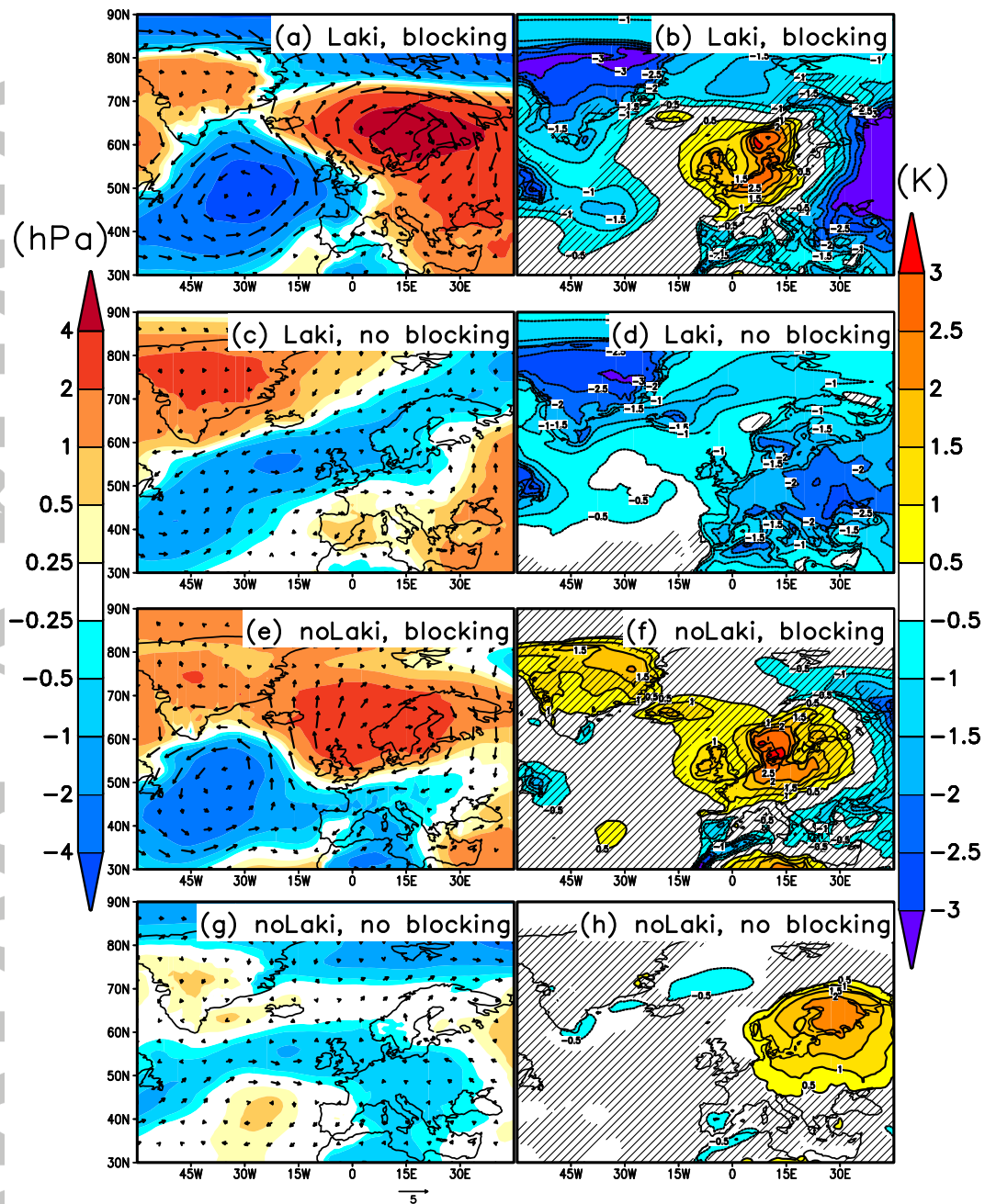
Figure 8. July 1783 sea level pressure anomalies (a, c, e, g shading; hPa) and 850 hPa wind anomalies (a, c, e, g vectors; m/s, with 5 m/s reference vector under panel g) and surface air temperature anomalies (b, d, f, h; K) for averages of: (a–b) Laki simulations with atmospheric blocking (ensemble members 1, 7, 10, 21, and 36; n = 5 simulations); (c–d) Laki simulations without atmospheric blocking (ensemble members 2–6, 8–9, 11–20, 22–35, and 37–40; n = 35 simulations); (e–f) noLaki simulations with atmospheric blocking (ensemble members 1, 7, 8, 36, and 38; n = 5 simulations); (g–h) noLaki simulations without atmospheric blocking (ensemble members 2–6, 9–35, 37, and 39–40; n = 35 simulations). Anomalies calculated with respect to the five years before the eruption. Hatching (b, d, f, h) represents areas < 90% significance using a two-tailed Student's *t*-test.
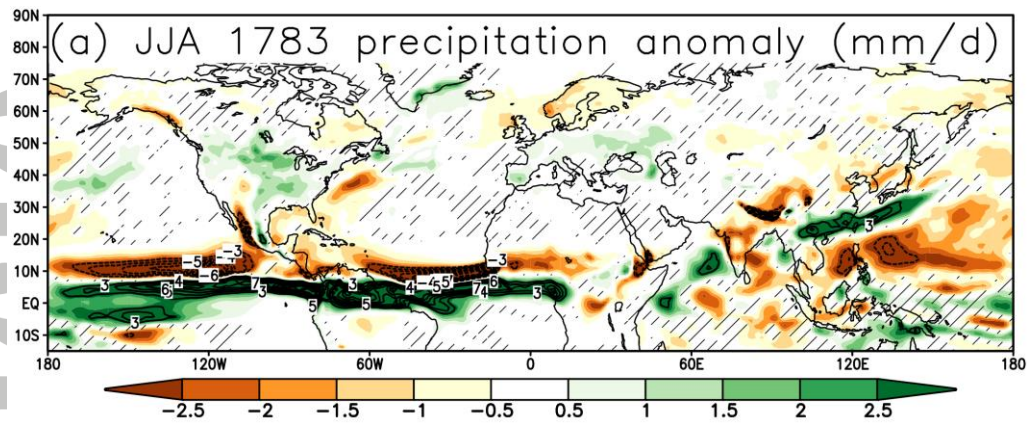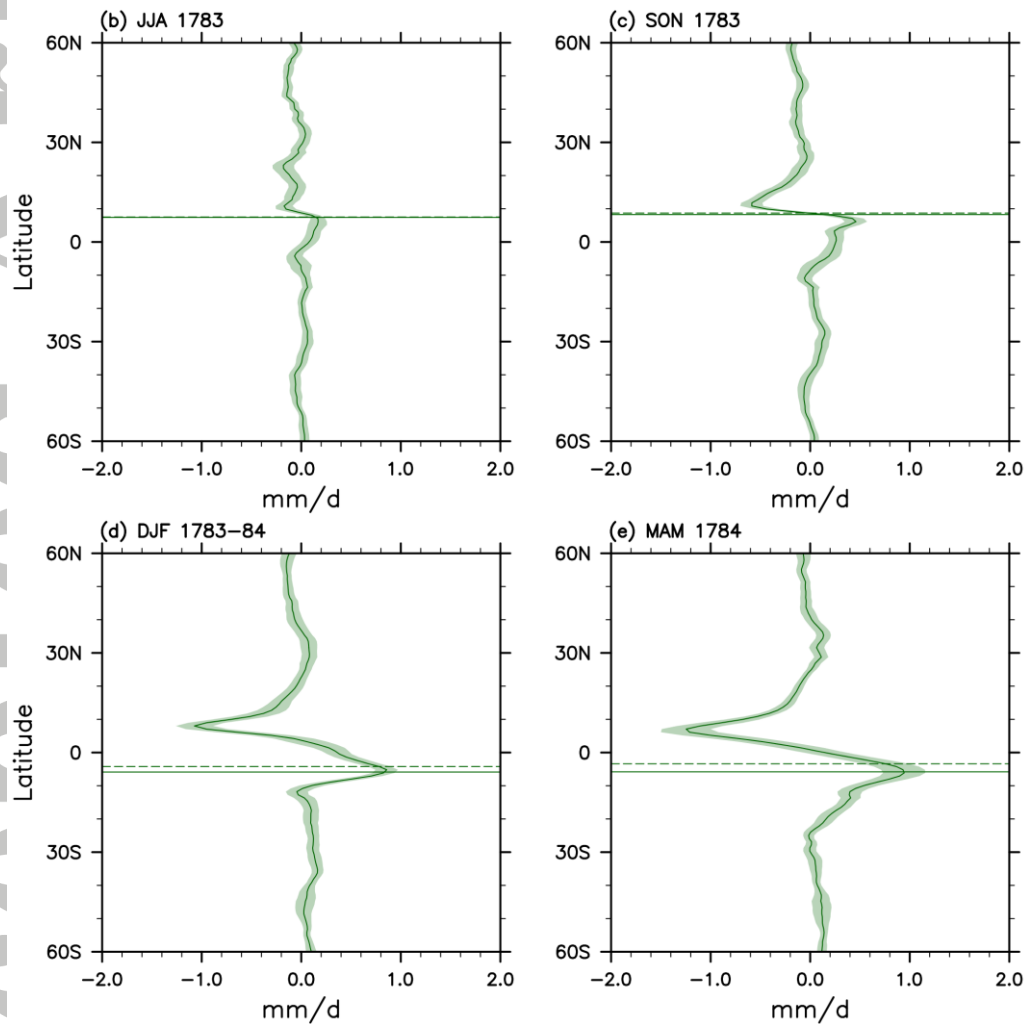
Figure 9. (a) JJA 1783 precipitation anomalies (mm/day) for the Laki ensemble average. Anomalies are calculated with respect to the five years before the eruption. Hatching represents areas < 95% significance using a two-tailed Student's *t*-test. ((b)-(e)) Zonal-mean precipitation anomalies for the Laki ensemble average. Shading represents the 95% confidence interval, the solid and dotted horizontal lines represent the ensemble-mean locations of the ITCZ for the noLaki and Laki ensembles, respectively.
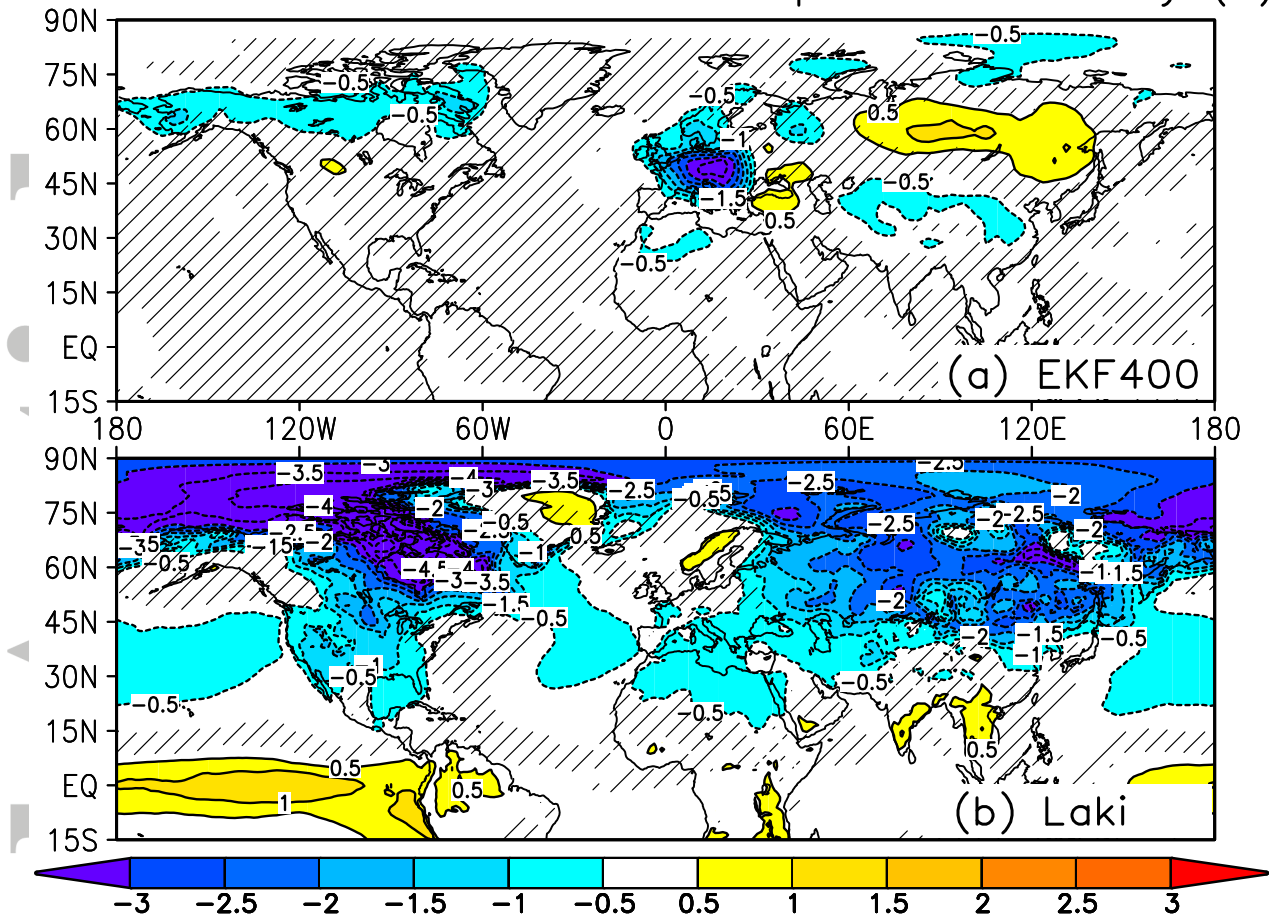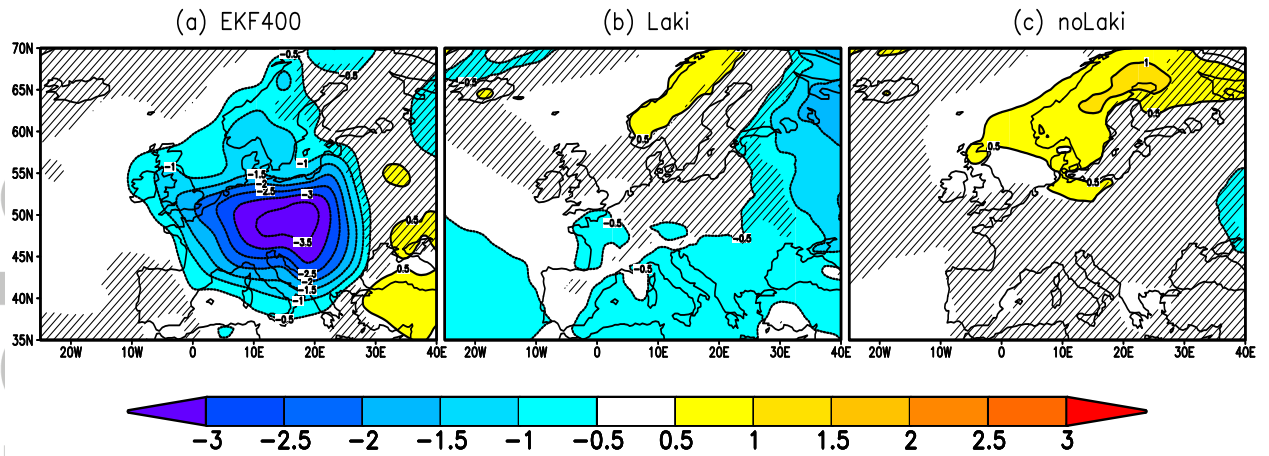
Figure 10. DJF 1783–1784 surface temperature anomalies (K) for (a) EKF400 reanalysis [*Franke et al.*, 2017] and (b) Laki ensemble average. Anomalies are calculated with respect to the five years before the eruption. Hatching represents areas < 95% significance using a two-tailed Student's *t*-test.

Figure 11. DJF 1783–1784 European surface temperature anomalies (K) for (a) EKF400 reanalysis [*Franke et al.*, 2017], (b) Laki ensemble average, and (c) noLaki ensemble average. Anomalies are calculated with respect to the five years before the eruption. Hatching represents areas < 95% significance using a two-tailed Student's *t*-test.

σ~T~ anomaly, EKF (1751−1800) minus HadCRUT4 (1951−2000) (%)
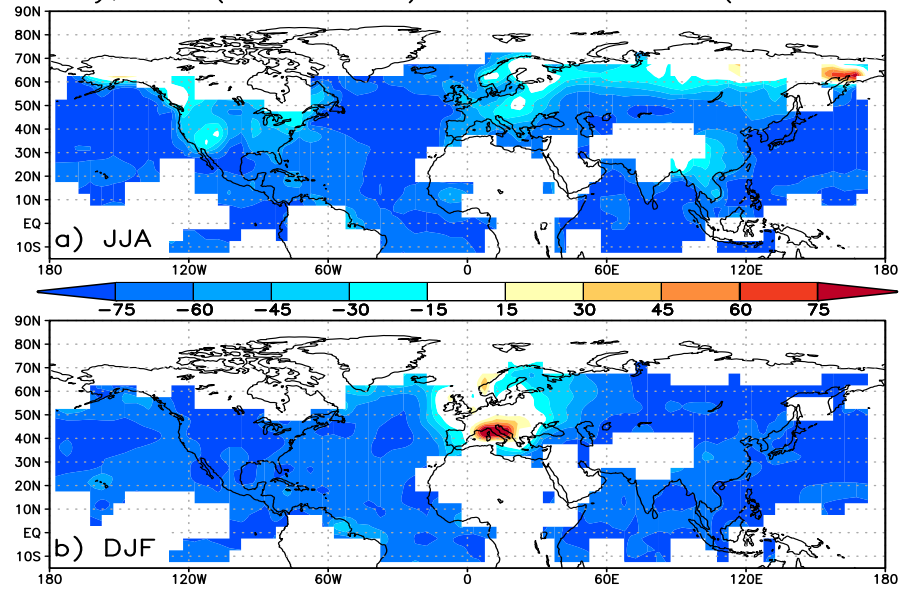
Figure 12. Difference in standard deviation (%) of temperature for (a) JJA and (b) DJF for the EKF400 reanalysis [*Franke et al.*, 2017] between 1751−1800 and 1951−2000 for HadCRUT4 [*Morice et al.*, 2012]. Blue shading indicates that variability in the 1751−1799 period is underestimated compared to the 1951−1999 period.

# Sea level pressure anomalies (hPa), Laki minus noLaki
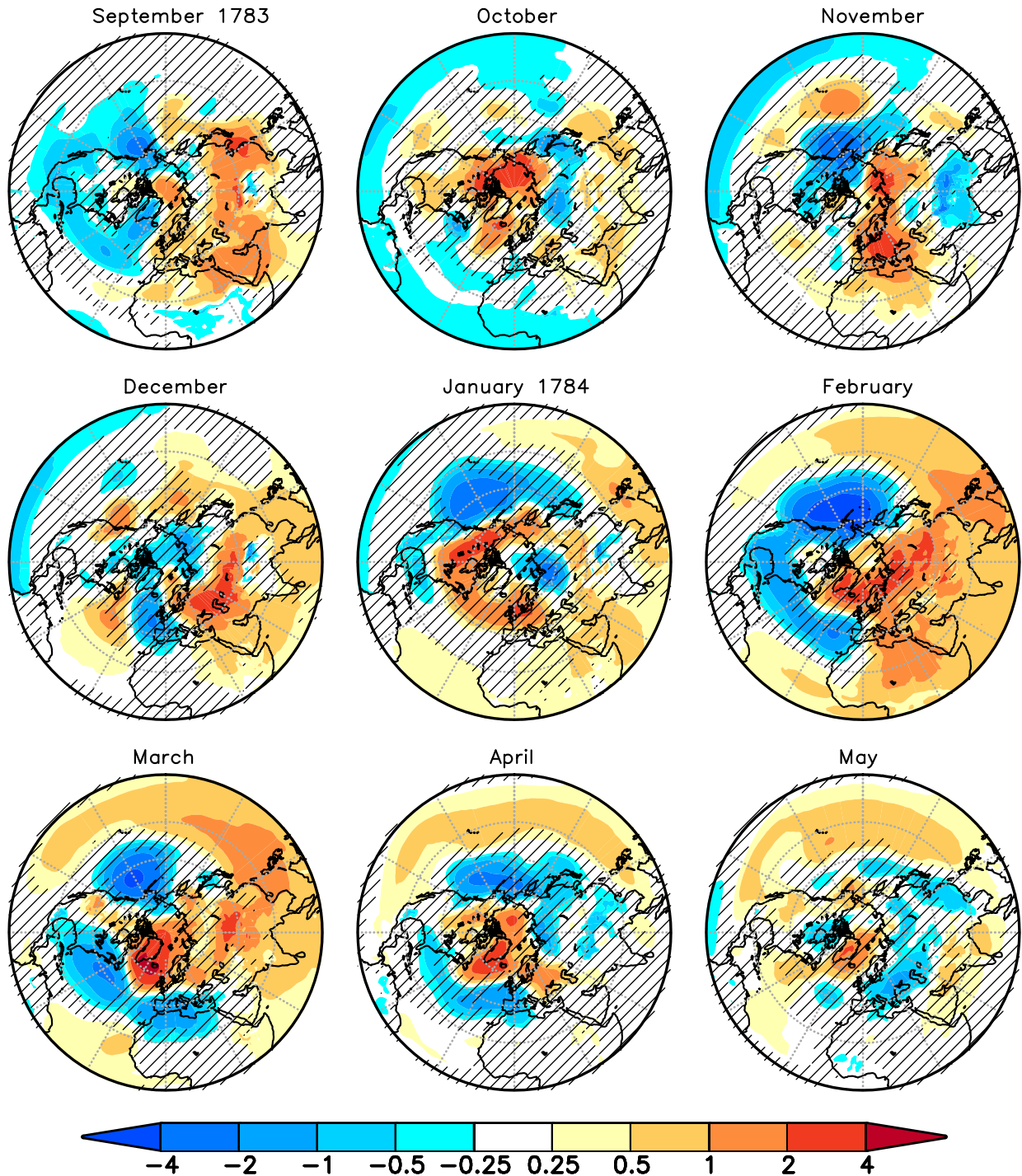
Figure 13. Northern Hemisphere sea level pressure anomalies (hPa) for the difference between the Laki and noLaki ensemble means. Hatching represents areas < 95% significance using a two-tailed Student's *t*-test.
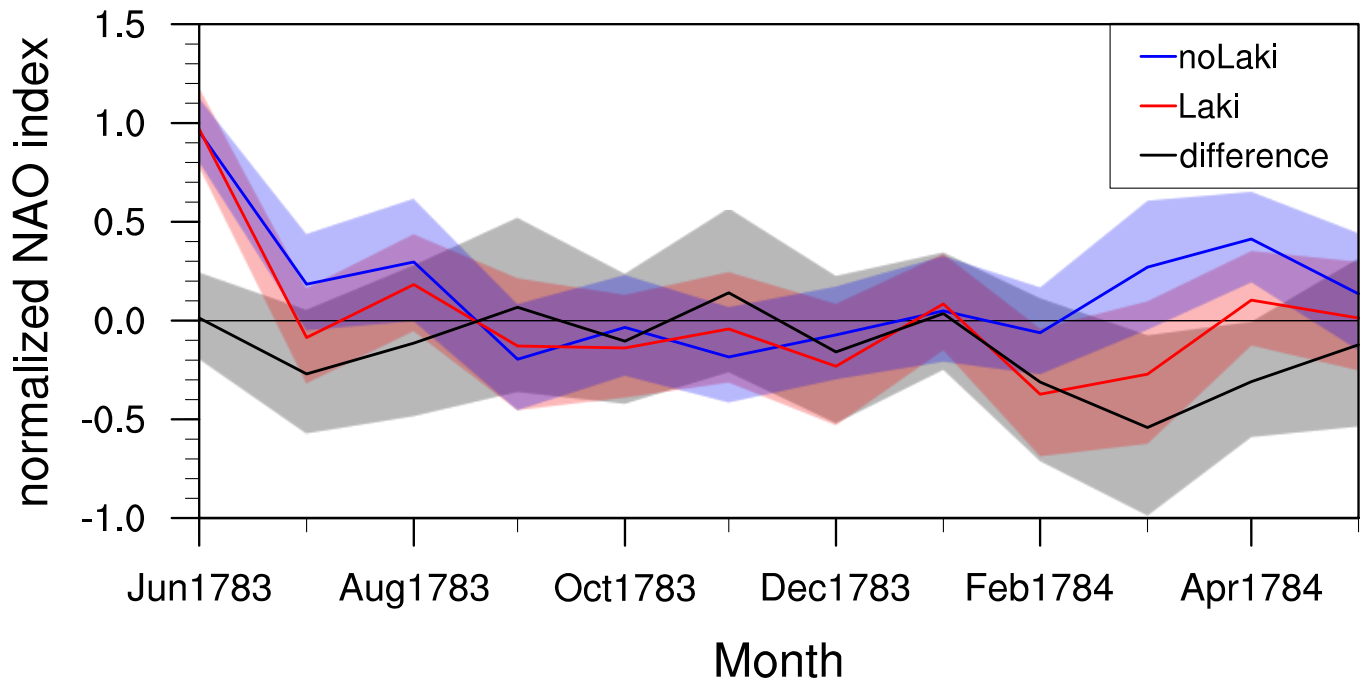
Figure 14. Normalized NAO index for noLaki ensemble mean (blue), Laki ensemble mean (red), and Laki minus noLaki (black). Shading represents the 95% confidence interval.
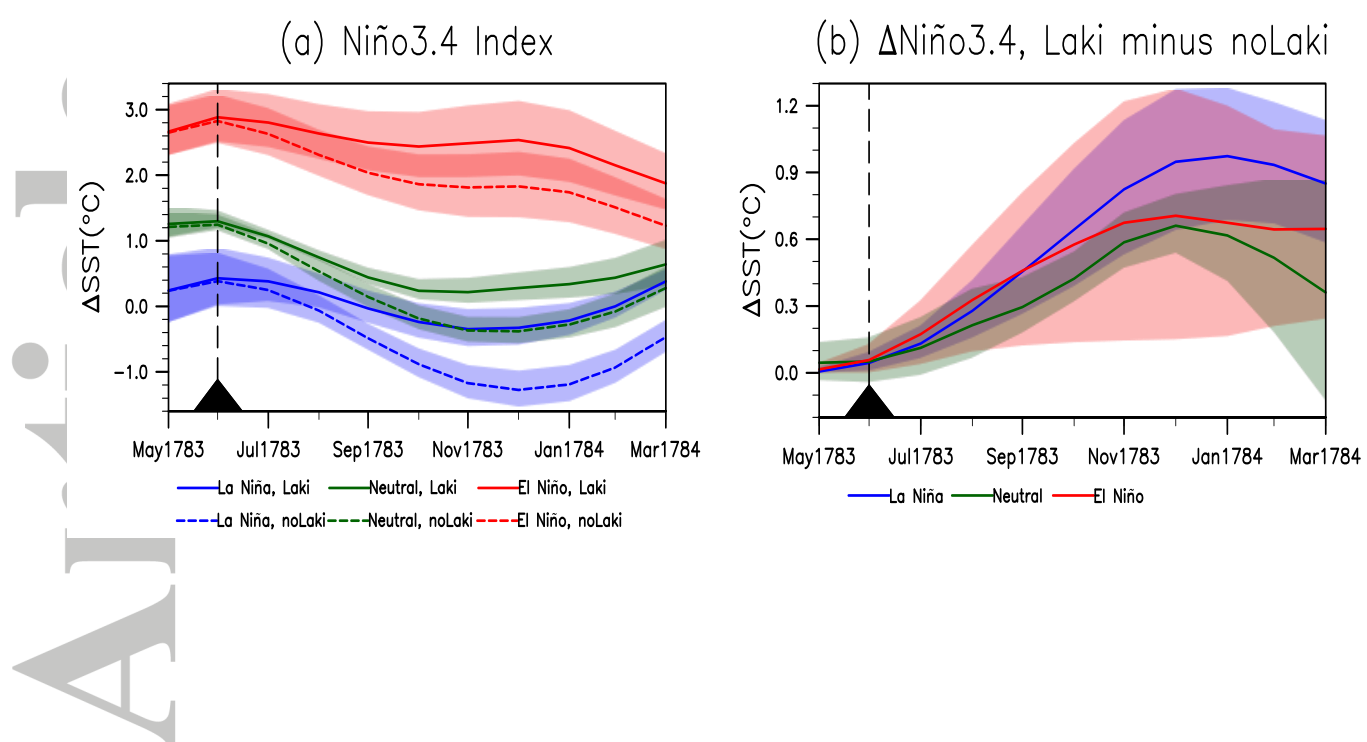
Figure 15. (a) Niño3.4 indices for the noLaki (dotted lines) and Laki (solid lines) ensembles for La Niña (blue), neutral (green), and El Niño (salmon) initial conditions. (b) Laki minus noLaki Nino 3.4 indices for La Niña (blue), neutral (green), and El Niño (salmon) initial conditions. Shading indicates 95% confidence interval.